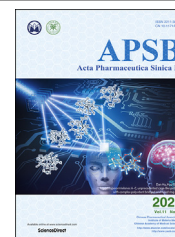




Chinese Pharmaceutical Association  
Institute of Materia Medica, Chinese Academy of Medical Sciences

Acta Pharmaceutica Sinica B

[www.elsevier.com/locate/apsb](http://www.elsevier.com/locate/apsb)  
[www.sciencedirect.com](http://www.sciencedirect.com)



ORIGINAL ARTICLE

# Ablation of Akt2 and AMPK $\alpha$ 2 rescues high fat diet-induced obesity and hepatic steatosis through Parkin-mediated mitophagy



Shuyi Wang<sup>a,b,c,†</sup>, Jun Tao<sup>d,†</sup>, Huaguo Chen<sup>a,†</sup>,  
Machender R. Kandadi<sup>c,e</sup>, Mingming Sun<sup>c,f</sup>, Haixia Xu<sup>f,g</sup>,  
Gary D. Lopaschuk<sup>h</sup>, Yan Lu<sup>i</sup>, Junmeng Zheng<sup>d,\*</sup>, Hu Peng<sup>a,\*</sup>,  
Jun Ren<sup>f,j,\*</sup>

<sup>a</sup>Department of Emergency, Shanghai Tenth People's Hospital, School of Medicine Tongji University, Shanghai 200072, China

<sup>b</sup>Shanghai University School of Medicine, Shanghai 200044, China

<sup>c</sup>University of Wyoming College of Health Sciences, Laramie, WY 82071, USA

<sup>d</sup>Department of Cardiovascular Surgery, Sun Yat-sen Memorial Hospital, Sun Yat-sen University, Guangzhou 510000, China

<sup>e</sup>Medprime Health Services LLC, Paris, TX 75460, USA

<sup>f</sup>Department of Cardiology, Shanghai Institute of Cardiovascular Diseases, Zhongshan Hospital Fudan University, Shanghai 200032, China

<sup>g</sup>Department of Cardiology, Affiliated Hospital of Nantong University, Nantong 226001, China

<sup>h</sup>Cardiovascular Research Centre, University of Alberta, Edmonton, Alberta T6G 2S2, Canada

<sup>i</sup>Key Laboratory of Metabolism and Molecular Medicine, Ministry of Education, Department of Endocrinology and Metabolism, Zhongshan Hospital Fudan University, Shanghai 200032, China

<sup>j</sup>Department of Laboratory Medicine and Pathology, University of Washington, Seattle, WA 98195, USA

Received 6 January 2021; received in revised form 4 June 2021; accepted 7 June 2021

\*Corresponding authors.

E-mail addresses: [zhengjunmeng@126.com](mailto:zhengjunmeng@126.com) (Junmeng Zheng), [1973denkepeng@tongji.edu.cn](mailto:1973denkepeng@tongji.edu.cn) (Hu Peng), [jren@uw.edu](mailto:jren@uw.edu) (Jun Ren).

<sup>†</sup>These authors made equal contributions to this work.

Peer review under responsibility of Chinese Pharmaceutical Association and Institute of Materia Medica, Chinese Academy of Medical Sciences.

<https://doi.org/10.1016/j.apsb.2021.07.006>

2211-3835 © 2021 Chinese Pharmaceutical Association and Institute of Materia Medica, Chinese Academy of Medical Sciences. Production and hosting by Elsevier B.V. This is an open access article under the CC BY-NC-ND license (<http://creativecommons.org/licenses/by-nc-nd/4.0/>).

**KEY WORDS**

Akt2;  
 AMPK;  
 Parkin;  
 High fat intake;  
 Obesity;  
 Steatosis;  
 Mitophagy;  
 FoxO1

**Abstract** Given the opposing effects of Akt and AMP-activated protein kinase (AMPK) on metabolic homeostasis, this study examined the effects of deletion of Akt2 and AMPK $\alpha$ 2 on fat diet-induced hepatic steatosis. *Akt2*–*Ampk $\alpha$ 2* double knockout (DKO) mice were placed on high fat diet for 5 months. Glucose metabolism, energy homeostasis, cardiac function, lipid accumulation, and hepatic steatosis were examined. DKO mice were lean without anthropometric defects. High fat intake led to adiposity and decreased respiratory exchange ratio (RER) in wild-type (WT) mice, which were ablated in DKO but not *Akt2*<sup>−/−</sup> and *Ampk $\alpha$ 2*<sup>−/−</sup> mice. High fat intake increased blood and hepatic triglycerides and cholesterol, promoted hepatic steatosis and injury in WT mice. These effects were eliminated in DKO but not *Akt2*<sup>−/−</sup> and *Ampk $\alpha$ 2*<sup>−/−</sup> mice. Fat diet promoted fat accumulation, and enlarged adipocyte size, the effect was negated in DKO mice. Fat intake elevated fatty acid synthase (FAS), carbohydrate-responsive element-binding protein (CHREBP), sterol regulatory element-binding protein 1 (SREBP1), peroxisome proliferator-activated receptor gamma coactivator 1-alpha (PGC-1 $\alpha$ ), peroxisome proliferator-activated receptor- $\alpha$  (PPAR $\alpha$ ), PPAR $\gamma$ , stearoyl-CoA desaturase 1 (SCD-1), phosphoenolpyruvate carboxykinase (PEPCK), glucose 6-phosphatase (G6Pase), and diglyceride *O*-acyltransferase 1 (DGAT1), the effect was absent in DKO but not *Akt2*<sup>−/−</sup> and *Ampk $\alpha$ 2*<sup>−/−</sup> mice. Fat diet dampened mitophagy, promoted inflammation and phosphorylation of forkhead box protein O1 (FoxO1) and AMPK $\alpha$ 1 (Ser<sup>485</sup>), the effects were eradicated by DKO. Deletion of Parkin effectively nullified DKO-induced metabolic benefits against high fat intake. Liver samples from obese humans displayed lowered microtubule-associated proteins 1A/1B light chain 3B (LC3B), Pink1, Parkin, as well as enhanced phosphorylation of Akt, AMPK (Ser<sup>485</sup>), and FoxO1, which were consolidated by RNA sequencing (RNAseq) and mass spectrometry analyses from rodent and human livers. These data suggest that concurrent deletion of Akt2 and AMPK $\alpha$ 2 offers resilience to fat diet-induced obesity and hepatic steatosis, possibly through preservation of Parkin-mediated mitophagy and lipid metabolism.

© 2021 Chinese Pharmaceutical Association and Institute of Materia Medica, Chinese Academy of Medical Sciences. Production and hosting by Elsevier B.V. This is an open access article under the CC BY-NC-ND license (<http://creativecommons.org/licenses/by-nc-nd/4.0/>).

**1. Introduction**

Non-alcoholic fatty liver disease (NAFLD) is characterized by hepatic steatosis that may progress into non-alcoholic steatohepatitis (NASH). NASH is associated with hepatic inflammation, fibrosis, and increased prevalence of cirrhosis and hepatocellular carcinoma<sup>1–3</sup>. NAFLD is closely associated with metabolic syndrome in obese or morbidly obese patients<sup>4,5</sup>. NAFLD presents with hepatic manifestations of metabolic syndrome including insulin resistance, obesity, and type 2 diabetes mellitus<sup>3–5</sup>. The incidence of NAFLD rises concurrently with obesity and type 2 diabetes, and is expected to become the leading cause of liver transplantation<sup>6</sup>. Understanding of etiology of NAFLD further explains the detrimental effects including insulin resistance, autophagy defect, inflammation, and fibrosis<sup>7–12</sup>. Minimal pharmacotherapy has been approved (licensed) for NAFLD to reverse or halt the progression of steatosis to NASH. Given the high incidence of NAFLD in obesity, one important issue for overweight or obese individuals may be the search for factors that trigger hepatic steatosis and ultimately liver injury<sup>11</sup>.

Metabolic disorders, particularly those involved in lipid metabolism, are important for the transition from metabolic syndrome to liver injury. Hepatic steatosis (lipid buildup) plays a complex and controversial role in the pathogenesis of NAFLD<sup>1,6,11</sup>. Increased levels of free fatty acids appear to be a major risk factor for NAFLD, and evidence has revealed that inhibition of triglyceride synthesis counters fatty acid-induced hepatic lipotoxicity in obesity<sup>13–15</sup>. A plethora of cytokines and cell-signaling molecules were identified that reveal the association between insulin signaling and NAFLD pathogenesis. Insulin resistance is cardinal to predispose hepatocytes to pathogenic

factors<sup>11,15</sup>. However, hepatic lipid accumulation was reported to be independent of insulin action, but rather relied on fatty acid substrate availability<sup>15,16</sup>. These findings denote a controversial role of hepatic lipid accumulation as an indicator or a causative mediator in metabolic diseases<sup>17</sup>. Among various signaling molecules in the regulation of hepatic insulin sensitivity and lipid metabolism, protein kinase B (Akt) and AMP-activated protein kinase (AMPK) remain the most prominent signals governing insulin sensitivity, lipid and energy metabolism<sup>18</sup>. Both genetic and high fat diet-induced obesity compromise Akt and AMPK regulation possibly due changes in nutrients, ATP, and proinflammatory cytokine levels<sup>19–21</sup>. Using genetically engineered murine models, distinct roles for Akt and AMPK were unveiled in hepatic lipogenesis and energy metabolism in high fat diet-induced insulin resistance and obesity<sup>22–25</sup>. Akt, in particular Akt2, is essential for activation of hepatic sterol regulatory element-binding protein 1c (SREBP1c), lipogenesis, and lipid accumulation in metabolic stress<sup>22,23</sup>. On the other hand, AMPK inhibits SREBP1c function, lipid accumulation, hepatic steatosis, and adiposity, which cause the metabolic benefits of drugs such as metformin<sup>24,26</sup>. Nonetheless, interactions between these two opposing signaling molecules in growth, lipid, and energy metabolism in adiposity and hepatic steatosis remain unclear.

To this end, we generated an *Akt2*–*Ampk $\alpha$ 2* double knockout (DKO) murine model to examine the impact of concurrent ablation of Akt2 and AMPK $\alpha$ 2 on high fat diet-induced obesity, hepatic steatosis, and inflammation. Given the established role of autophagy and mitochondrial autophagy (aka mitophagy) in adiposity, hepatic steatosis, and injury<sup>8,10,17,27</sup>, and the apparent reciprocal regulatory modality of Akt and AMPK on autophagy and mitophagy<sup>27,28</sup>, mitophagy was examined in high fat diet-

induced in obesity and hepatic steatosis. Our results depict concurrent deletion of Akt2 and AMPK $\alpha$ 2 rescued high fat diet intake-induced loss of mitophagy molecule Parkin but not FUN14 domain-containing protein 1 (FUNDC1) and BCL2/adenovirus E1B 19 kDa protein-interacting protein-3 (BNIP3). To this end, an Akt2–Ampk $\alpha$ 2–Parkin triple knockout (TKO) murine line was generated to further discern the role of Parkin. In support of our experimental findings, RNA sequencing (RNAseq), mass spectrometry, and immunoblot analyses from obese rodent and human liver samples all depicted prominent roles for gene ontology terms related to cell signaling of Akt, AMPK, autophagy, mitophagy, and lipid metabolism in liver injury.

## 2. Materials and methods

### 2.1. Human samples and liquid chromatography–tandem mass spectrometry (LC–MS/MS) analysis

Liver specimens were obtained from liver transplants from lean and obese patients (Supporting Information Table S1) under an approved protocol (No. B2020-127R) by Zhongshan Hospital Fudan University Ethics Committee (Shanghai, China) and were carried out in accordance with the Declaration of Helsinki for experiments involving humans. LC–MS/MS data acquisition of human liver samples was carried out on an Orbitrap Exploris 480 mass spectrometer coupled with an Easy-nLC 1200 system (Thermo Scientific, USA)<sup>27</sup>. Peptides were first loaded onto a C18 trap column (75  $\mu$ m  $\times$  2 cm, 3  $\mu$ m particle size, 100 Å pore size, Thermo Scientific) and then separated in a C18 analytical column (75  $\mu$ m  $\times$  250 mm, 3  $\mu$ m particle size, 100 Å pore size, Thermo). Mobile phase A (0.1% formic acid) and B (80% acetonitrile, 0.1% formic acid) were used to establish the separation gradient. A constant flow rate was set at 300 nL/min. For data dependent acquisition (DDA) mode analysis, each scan cycle consisted of one full-scan mass spectrum followed by 20 MS/MS events. Higher energy collision dissociation (HCD) was set to 32. Isolation window for precursor selection was set to 1.2 Da. Former target ion exclusion was set for 30 s. MS raw data were analyzed with MaxQuant (V1.6.6) using the Andromeda database search algorithm. Spectra files were searched against the UniProt human protein database, and search results were filtered with 1% false discovery rate (FDR) at both protein and peptide levels. Proteins denoted as decoy hits, contaminants, or only identified by sites were removed, and the remaining proteins were used for further analysis.

### 2.2. mRNA sequencing (mRNA-Seq)

mRNA-Seq was done by Novogene (Beijing, China) and Cloudseq Biotech Inc. (Shanghai, China). Standard Illumina protocols were used for sequencing after preparation of mRNA-seq library. RNAs were isolated from livers from adult *db/db* obese mice or rats (Nanjing Biomedical Research Institute of Nanjing University, Nanjing, China) following 45% high fat diet intake for 20 weeks using TRIzol reagent (Invitrogen, Carlsbad, CA, USA). Twelve-week-old *db/db* mice or rats were housed at 21  $\pm$  1 °C with a humidity of 55%  $\pm$  10% and a 12-h/12-h light/dark cycle. To remove any contaminating genomic DNA, RNase-free DNase I (New England Biolabs, MA, USA) was applied to isolated RNAs. Dynabeads oligo (dT) (Invitrogen) were used to extract mRNA, and double-stranded complementary DNAs (cDNAs) were synthesized

using Superscript II reverse transcriptase (Invitrogen) and random hexamer primers. To create mRNA-seq library, cDNAs were fragmented by nebulization and standard Illumina protocol was followed thereafter. For data analysis, base calls performed using CASAVA Reads (version 1.8.2 software, Illumina, CA, USA) were aligned to genome using split read aligner TopHat (version 2.0.7, Ontario, Canada) and Bowtie2 (<http://bowtie-bio.sourceforge.net/index.shtml>). HTSeq (<http://www-huber.embl.de/HTSeq>) was used for estimation of their abundance<sup>29</sup>.

### 2.3. Functional analysis of differentially expressed proteins using bioinformatics

Gene Ontology (GO) and Kyoto Encyclopedia of Genes and Genomes (KEGG) pathway enrichment analyses were performed using the OmicShare tools, a free online platform for data analysis (<http://www.omicshare.com/tools>).

### 2.4. Akt2 and Ampk $\alpha$ 2 knockout mice, generation of Akt2–Ampk $\alpha$ 2 double or Akt2–Ampk $\alpha$ 2–Parkin triple knockout mice, and high fat diet feeding

All animal procedures were approved by the Animal Care and Use Committee at the Zhongshan Hospital Fudan University (Shanghai, China) and University of Wyoming (Laramie, WY, USA). Akt2 knockout (Akt2<sup>−/−</sup>) mice were obtained from Dr. Morris J. Birnbaum at the University of Pennsylvania (Philadelphia, PA, USA) and Ampk $\alpha$ 2 knockout (Ampk $\alpha$ 2<sup>−/−</sup>) mice were generated and characterized by Dr. Benoit Viollet at the Institute Cochin, Université Paris Descartes, CNRS (UMR 8104) in Paris, France<sup>30,31</sup>. Akt2<sup>−/−</sup> and Ampk $\alpha$ 2<sup>−/−</sup> mice (both on C57BL/6J background) were bred to generate DKO mice. To produce Akt2<sup>−/−</sup>Ampk $\alpha$ 2<sup>−/−</sup>–Parkin<sup>−/−</sup> (Prk<sup>−/−</sup>) triple knockout (TKO) mice, the DKO mice were crossed with Prk<sup>−/−</sup> mice to generate heterozygotes, which were further crossed to produce TKO mice. Global Prk<sup>−/−</sup> mice were purchased from the Jackson Laboratory (B6.129S4-Parktm1Shn/J, stock number 006582). To confirm genotypes, genomic DNA prepared from tail snips was analyzed using PCR (Supporting Information Table S2). Mice were housed under temperature-controlled conditions (22  $\pm$  2 °C), humidity (55%  $\pm$  5%), and a 12 h/12 h light–dark circadian cycle with access to food and water *ad libitum*. Five-week-old male Akt2<sup>−/−</sup> or Ampk $\alpha$ 2<sup>−/−</sup>, DKO, or TKO mice, and their wild-type (WT) littermates were placed on a low fat (Cat. D12450B, 10% calories from fat, 3.91 kcal/g) or high fat (Cat. D12451, 45% calories from fat, 4.83 kcal/g; Research Diets, New Brunswick, NJ, USA) diet for 20 weeks<sup>25,32</sup>. In another cohort of study, five-week-old male Prk<sup>−/−</sup> or TKO mice and their WT littermates were placed on a low fat or high fat diet for 20 weeks. Food intake was recorded using a lab scale. Body fat composition (% lean and fat mass) was measured at the end of 20-week feeding period using a Dual Energy X-ray Absorptiometry (GE Lunar Prodigy™ 8743; Madison, WI, USA). Animal sample size was determined using power analysis.

### 2.5. Intraperitoneal glucose tolerance test (IPGTT), serum lipid, and insulin measurement

Mice fasted for 12 h and then were given an intraperitoneal injection of glucose (2 g/kg body weight). Blood samples were collected from the tail vein immediately before glucose challenge, as well as 15, 30, 60, and 120 min thereafter. Serum glucose levels were

determined using an Accu-Chek III glucose analyzer (Roche, Germany). Area under curve (AUC) was calculated using trapezoidal analysis<sup>32</sup>. Serum levels of insulin, triglycerides, and cholesterol were measured using commercial kits (BioVision, Inc., Mountain View, CA, USA; EMD Millipore Corp., Billerica, MA, USA)<sup>32</sup>. Serum levels of aspartate aminotransferase (AST) and alanine aminotransferase (ALT) were determined using colorimetric assay kits from BioVision per manufacturer's instructions<sup>33</sup>.

## 2.6. Metabolic measurement

A Comprehensive Laboratory Animal Monitoring System (CLAMSTM, Columbus Instruments, Columbus, OH, USA) was used to monitor global metabolism. Mice were housed in individual CLAMS metabolic cages with access to food and water *ad libitum*. Following acclimation, metabolic parameters including carbon dioxide production (VCO<sub>2</sub>), oxygen consumption (VO<sub>2</sub>), respiratory exchange ratio (RER = VCO<sub>2</sub>/VO<sub>2</sub>), heat production [(3.815 + 1.232 × RER) × VO<sub>2</sub> × 1000], and physical activity (horizontal beam breaks) were recorded every 12 min over a period of 24 h (light phase: 7:00 am–7:00 pm; dark phase: 7:00 pm–7:00 am)<sup>34</sup>.

## 2.7. Hepatic triglycerides

Hepatic triglyceride levels were measured using a colorimetric kit from BioVision. Following anesthesia (ketamine 80 mg/kg and xylazine 12 mg/kg, ip), liver tissues were collected and were homogenized before being heated in 5% NP-40 solution (90 °C for 5 min). Solubilized triglyceride lysate was centrifuged and supernatants were employed for triglyceride assay using a Spectra Max 190 Spectrophotometer (Molecular Devices, Sunnyvale, CA, USA)<sup>35</sup>.

## 2.8. Liver and adipose tissue histology, oil red O staining

Lipid droplet accumulation was determined using oil red O staining. Following anesthesia, livers and white and brown adipose tissues were collected and placed in 10% neutral-buffered formalin at room temperature for 24 h. All samples were embedded in paraffin, cut in 7- $\mu$ m sections, and were used for hematoxylin and eosin (H&E) staining. For oil red O staining, samples were sliced and snap-frozen in isopentane-cooled liquid nitrogen and were cut into 10- $\mu$ m sections using a cryostat. Sections were fixed with 10% neutral-buffered formalin, rinsed with 60% isopropanol and stained with diluted oil red O solution (0.5 g oil red O powder in 100 mL isopropanol then diluted by 1.66 times) for 20 min prior to imaging using an Olympus BX-51 microscope (Tokyo, Japan)<sup>36</sup>.

## 2.9. Western blot analysis

Tissues were homogenized in a RIPA lysis buffer and centrifuged at 13,000 × g for 20 min at 4 °C. Sample (30–50  $\mu$ g protein/lane) were then separated on sodium dodecyl sulfate (SDS)-polyacrylamide gels in a minigel apparatus (Mini-PROTEAN II, Bio-Rad, Hercules, CA, USA) and were transferred to nitrocellulose membranes. Membranes were blocked and were incubated overnight at 4 °C with anti-fatty acid synthase (FAS, 1:1000), anti-phospho-acetyl-CoA carboxylase (ACC, Ser<sup>79</sup>, 1:1000), anti-ACC (1:1000), anti-carbohydrate-responsive element-binding protein (CHREBP, 1:1000), anti-sterol regulatory element-binding protein 1c (SREBP1c, 1:1000), anti-

peroxisome proliferator-activated receptor gamma coactivator 1-alpha (PGC-1 $\alpha$ , 1:1000), anti-peroxisome proliferator-activated receptor- $\alpha$  (PPAR $\alpha$ , 1:1000), anti-PPAR $\gamma$  (1:1000), anti-stearoyl-CoA desaturase 1 (SCD-1, 1:1000), anti-diglyceride O-acyltransferase 1 (DGAT1, 1:500), anti-phosphoenolpyruvate carboxykinase (PEPCK, 1:1000), anti-glucose 6-phosphatase (G6Pase, 1:1000), anti-tumor necrosis factor- $\alpha$  (TNF- $\alpha$ , 1:500), anti-interleukin-6 (IL-6, 1:250), anti-microtubule-associated proteins 1A/1B light chain 3B (LC3B, 1:1000), anti-p62 (1:1000), anti-outer mitochondrial membrane 20 (TOM20, 1:1000), anti-Parkin (1:1000), anti-FUNDC1 (1:1000), anti-BNIP3 (1:1000), anti-phospho-forkhead box protein O1 (FoxO1, Ser<sup>256</sup>, 1:1000), anti-FoxO11 (1:1000), anti-Akt (1:1000), anti-Akt1 (1:1000), anti-Akt2 (1:1000), anti-Akt3 (1:1000), anti-phospho-Akt (Ser<sup>473</sup>, 1:1000), anti-AMPK (1:1000), anti-AMPK $\alpha$ 1 (1:1000), anti-AMPK $\alpha$ 2 (1:1000), anti-phospho-AMPK (Thr<sup>172</sup>, 1:1000), anti-phospho-AMPK (Ser<sup>485</sup>, 1:1000), and anti-glyceraldehyde 3-phosphate dehydrogenase (GAPDH) or anti- $\alpha$ -tubulin (loading controls, 1:1000) antibodies. All antibodies were purchased from Cell Signaling Technology (Danvers, MA, USA) or Abcam (Cambridge, MA, USA). Gel blots were incubated for 1 h with horseradish peroxidase (HRP)-conjugated secondary antibody (1:5000) and were quantified using the Quantity One software (Bio-Rad)<sup>35</sup>.

## 2.10. RNA isolation and gene expression

mRNA samples were isolated and purified following the instruction of Trizol Reagent (Invitrogen). cDNA was synthesized using the iScriptTM cDNA Synthesis Kit (Bio-Rad) and was mixed with SsoAdvanced Universal SYBR Green Supermix (Bio-Rad) and primers (sequences provided in Table S2). Reactions were executed using a CFX96TM RT-PCR detection system (Bio-Rad). The mRNA levels were expressed relative to *Gapdh*<sup>37</sup>.

## 2.11. HepG2 cell culture, treatment, and RNA interference

Small interfering RNA (siRNA) against *AMPK*, *AKT2* (On-TARGET plus SMART pool siRNA), or control non-targeting siRNA was obtained from Dharmacon (Lafayette, CO, USA). HepG2 cells (used for better siRNA efficacy) were grown in the Dulbecco's modified Eagle's medium (DMEM) supplemented with 10% fetal bovine serum (FBS) (Gibco, Grand Island, NY, USA), and 1% penicillin and streptomycin and maintained in 95% air and 5% CO<sub>2</sub> at 37 °C. Cells were grown to 70% confluence prior to transfection with siRNA (100 nmol/L) in DMEM using the Dharma FECT 1 transfection reagent. The *AMPK* siRNA sequence was: 5'-CCCTTCCTATGATGCTAACG-3' (forward); 5'-AGAACTCACTGGCTTGGTTC-3' (reverse)<sup>38</sup>. The *AKT2* siRNA sequence was: 5'-GCCTGAGGTGCTAGAGGACAAT-3' (forward); 5'-GAAGCCGATCTCCTCCATAAGA-3' (reverse)<sup>39</sup>. After 72 h of transfection, cells were exposed to palmitate acid (0.5 mmol/L)<sup>40</sup> in the presence or absence of the autophagy inhibitor 3-methyladenine (3-MA, 10 mmol/L)<sup>41</sup> or the FoxO1 inhibitor AS1842856 (100 nmol/L)<sup>42</sup> for 72 h followed by fixation.

## 2.12. Evaluation of lipid accumulation and triglyceride content in vitro

Lipid accumulation was evaluated using oil red O staining. HepG2 cells were fixed with ice-cold 10% formalin for 30 min. Cells were washed three times with sterile phosphate-buffered saline (PBS) and were stained with oil red O for 20 min as described above.

Images were taken through light microscopy (400 $\times$ ) and the absorbance for oil Red O dye eluted by isopropanol was measured at 530 nm wavelength using the Spectra Max 190 Microplate Spectrophotometer (molecular devices)<sup>43,44</sup>. Levels of triglycerides from cell lysates were determined using a biochemistry assay kit (Abcam)<sup>45</sup>.

### 2.13. Statistical analysis

Data were shown as mean  $\pm$  standard error of the mean (SEM). The Shapiro–Wilk normality test was used to examine distribution of experimental data. Statistical significance ( $P < 0.05$ ) was estimated using analysis of variance (ANOVA) followed by a Tukey's *post hoc* analysis. Due to the cost and potential mortality issues, not every single mouse from each group was subjected to metabolic cage, intraperitoneal glucose tolerance test (IGTT), and dual energy X-ray absorptiometry (DEXA) analyses, thus creating a smaller sample size for these indices.

## 3. Results

### 3.1. Changes in cell signaling pathways in livers from diet-induced rodent and human obesity

To discern possible biological processes and cell signaling pathways involved in liver injury in obesity, liver tissues were collected from adult Sprague–Dawley rats fed with high fat diet for 20 weeks and adult *db/db* leptin receptor deficient obese mice, prior to RNAseq analysis. As shown in Fig. 1, comparison between lean and obese rodents identified 1618 (rats) and 1131 (mice) genes with statistically significant differential expression [including 939 (rats) and 692 (mice) up-regulated and 679 (rats) and 439 (mice) down-regulated genes,  $P < 0.05$ ]. A hierarchical clustering of the most highly regulated genes showed distinct patterns between the lean and obese groups (Fig. 1a, rats; Fig. 1e, mice). Biological function analysis for differentially expressed genes revealed that GO terms associated with “metabolic processes” were notably changed (Fig. 1b, rats; Fig. 1f, mice). Cellular processes of KEGG class analysis revealed that obesity (diet-induced or *db/db* genetic) affected proteins involved in autophagy and mitophagy processes (Fig. 1c, rats; Fig. 1g, mice). Environmental information processing of KEGG class analysis indicated that obesity-regulated proteins were enriched in phosphoinositide 3-kinases (PI3K)–Akt, AMPK, and FoxO signaling pathways (Fig. 1d, rats; Fig. 1h, mice). To confirm altered proteins in obesity, lean and obese human liver tissues were examined using LC–MS/MS. The 406 differentially expressed proteins were found (including 131 up-regulated and 275 down-regulated; fold change  $> 2$ ). The most highly regulated proteins were displayed with distinct patterns in these two human groups (Fig. 2a). Similar to RNAseq findings from rodents, biological process enrichment analyses of human samples revealed that GO terms associated with “metabolic processes” were notably altered (Fig. 2b). Cellular processes of KEGG class analysis showed that obesity-regulated proteins were enriched in autophagy and mitophagy processes (Fig. 2c). Environmental information processing of KEGG class analysis indicated that obesity-regulated proteins were clustered in PI3K–Akt, AMPK, and FoxO signaling pathways (Fig. 2d). These results indicate a possible role of

PI3K–Akt, AMPK, FoxO, autophagy and mitophagy signaling in obesity-associated liver injury.

### 3.2. Biometric parameters and glucose sensitivity

As shown in Supporting Information Fig. S1a and S1b, DKO of both *Akt2* and *Ampk $\alpha$ 2* had little effect on Akt1, Akt3, and AMPK $\alpha$ 1 in hearts, livers, and muscles. Levels of pan-Akt and -AMPK were significantly downregulated in all tissues from DKO mice (except Akt levels in the hearts and muscles). High fat diet intake significantly increased body weight in WT, *Akt2*<sup>−/−</sup> and *Ampk $\alpha$ 2*<sup>−/−</sup> mice starting from 12 weeks of diet feeding. This effect was absent in DKO mice. Food intake was comparable among all groups (Fig. 3a–c). High fat diet intake overtly compromised glucose sensitivity in WT mice, the effect of which was absent in DKO but not *Akt2*<sup>−/−</sup> and *Ampk $\alpha$ 2*<sup>−/−</sup> mice, as demonstrated by the IPGTT test (Fig. 3d and e). Along the same line, high fat diet intake increased serum insulin levels in WT mice, the effect of which was absent in DKO but not *Akt2*<sup>−/−</sup> and *Ampk $\alpha$ 2*<sup>−/−</sup> mice (Fig. 3f). The 5-month high fat diet intake significantly lowered lean mass percentage (without affecting absolute lean mass) and increased both absolute and normalized fat mass in WT mice, the effect of which was absent in DKO but not *Akt2*<sup>−/−</sup> and *Ampk $\alpha$ 2*<sup>−/−</sup> mice (Fig. 3g–j).

### 3.3. Global metabolism, hepatic steatosis and liver function

To discern the possible mechanisms behind fat diet intake- and DKO-induced biometric and metabolic action, CLASM metabolic cage was employed to monitor global metabolism over a 24-h cycle. Our data revealed that high fat intake visibly lowered O<sub>2</sub> consumption, CO<sub>2</sub> production and RER in WT mice, the effect of which was absent in DKO but not *Akt2*<sup>−/−</sup> and *Ampk $\alpha$ 2*<sup>−/−</sup> mice. Ablation of *Akt2*, AMPK $\alpha$ 2, or both, had little effects on O<sub>2</sub> consumption, CO<sub>2</sub> production, and RER under low fat intake (Fig. 4a–i). Heat production and total activity were not notably affected by high fat intake, ablation of *Akt2*, AMPK $\alpha$ 2, or both (Fig. 4j–o). To evaluate high fat diet-induced hepatic steatosis and liver injury, if any, hepatic morphology, levels of triglycerides, AST, ALT, and cholesterol were assessed. Compared to normal lobular architecture in low fat-fed mice, high fat diet intake induced a microvesicular lipid accumulation, especially in centrilobular zone and hepatocyte ballooning with rarefaction of hepatocyte cytoplasm (Fig. 5a). Oil red O staining revealed hepatic steatosis following high fat intake (Fig. 5b). High fat intake also significantly increased liver weight (Fig. 5c and Supporting Information Fig. S2a), liver triglyceride content (Fig. 5d), serum levels of AST (Fig. 5e), ALT (Fig. 5f), triglycerides (Fig. 5g), and cholesterol (Fig. 5h). These signs of hepatic steatosis, were abrogated in DKO mice but not *Akt2*<sup>−/−</sup> and *Ampk $\alpha$ 2*<sup>−/−</sup> mice. Ablation of *Akt2*, AMPK $\alpha$ 2, or both, did not display any effects on hepatic morphology, triglyceride or serum profiles of liver injury and dyslipidemia in the face of low fat diet intake (Fig. 5a–h). Moreover, our data revealed enlarged size of adipocytes, brown adipose tissues, white adipose tissues (inguinal, epididymal, and retroperitoneal), and ectopic fat accumulation (in the form of triglycerides) in muscles in high fat diet-fed WT mice. The effects of which were removed in DKO but not *Akt2*<sup>−/−</sup> and *Ampk $\alpha$ 2*<sup>−/−</sup> mice following high fat intake (Supporting Information Fig. S2b–S2g). Ablation of *Akt2*, AMPK $\alpha$ 2, or both, did not display any discernible effects on these biometric and metabolic parameters under low fat diet intake (Fig. S2).

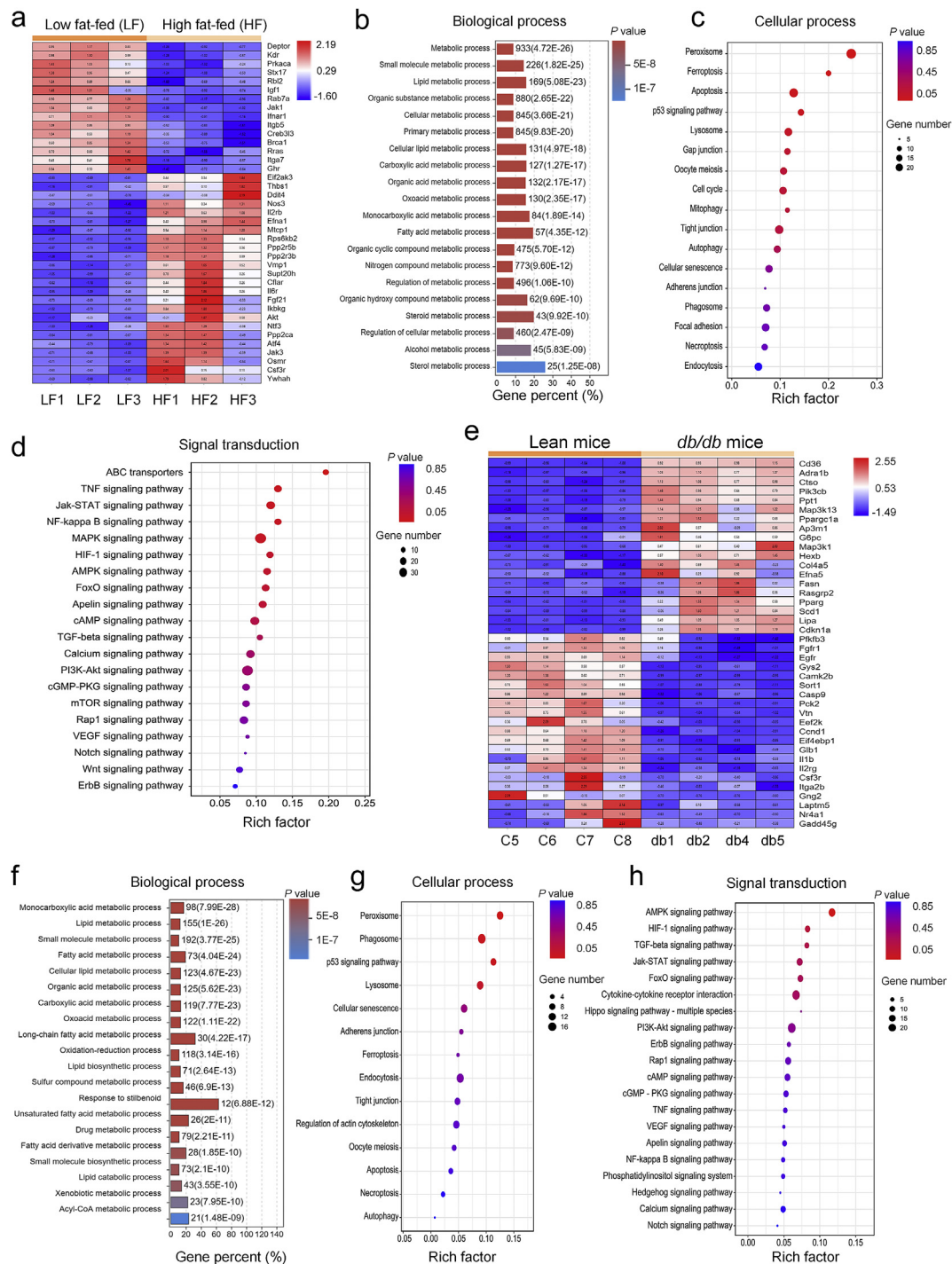


**Figure 1** High fat diet intake and leptin receptor deficient obesity-modulated molecular events and cell signaling pathways in livers. Liver tissues of rats fed high fat diet for 20 weeks (a–d) or *db/db* obese and C57BL/6J lean mice (e–h) were subjected to RNAseq analysis. (a and e) Heatmap displays significantly regulated genes in signaling pathways of PI3K–Akt, AMPK, and FoxO, as well as cellular processes of autophagy and mitophagy in rat (a) and mice (e), respectively. (b and f) GO analysis was conducted with all altered genes, and 20 highest-ranking biological process terms are shown, rat (b) and mice (f), respectively; (c and g) KEGG pathway analyses of all significantly regulated genes were performed, and the enrichment for cellular process of KEGG pathway is shown using bubble plot, rat (c) and mice (g), respectively; (d and h) Bubble plot shows the enrichment for signal transduction of KEGG pathway, rat (d) and mice (h), respectively.

### 3.4. Hepatic lipid metabolism

To evaluate the impact of DKO on high fat diet-induced hepatic lipid metabolism, lipid synthesis, uptake, and transport genes were evaluated using RT-PCR and Western blot analyses. High fat diet

intake clearly upregulated mRNA levels of the key enzyme for fatty acid synthesis including *Fas*, transcription factors in lipogenesis including *Chrebp* and *Srebp1*, essential enzymes involved in lipid metabolism such as *Pgc-1 $\alpha$*  and *Ppar $\alpha$* , lipid storage such as *Ppar $\gamma$* , unsaturated fatty acid synthesis catalyzing enzymes

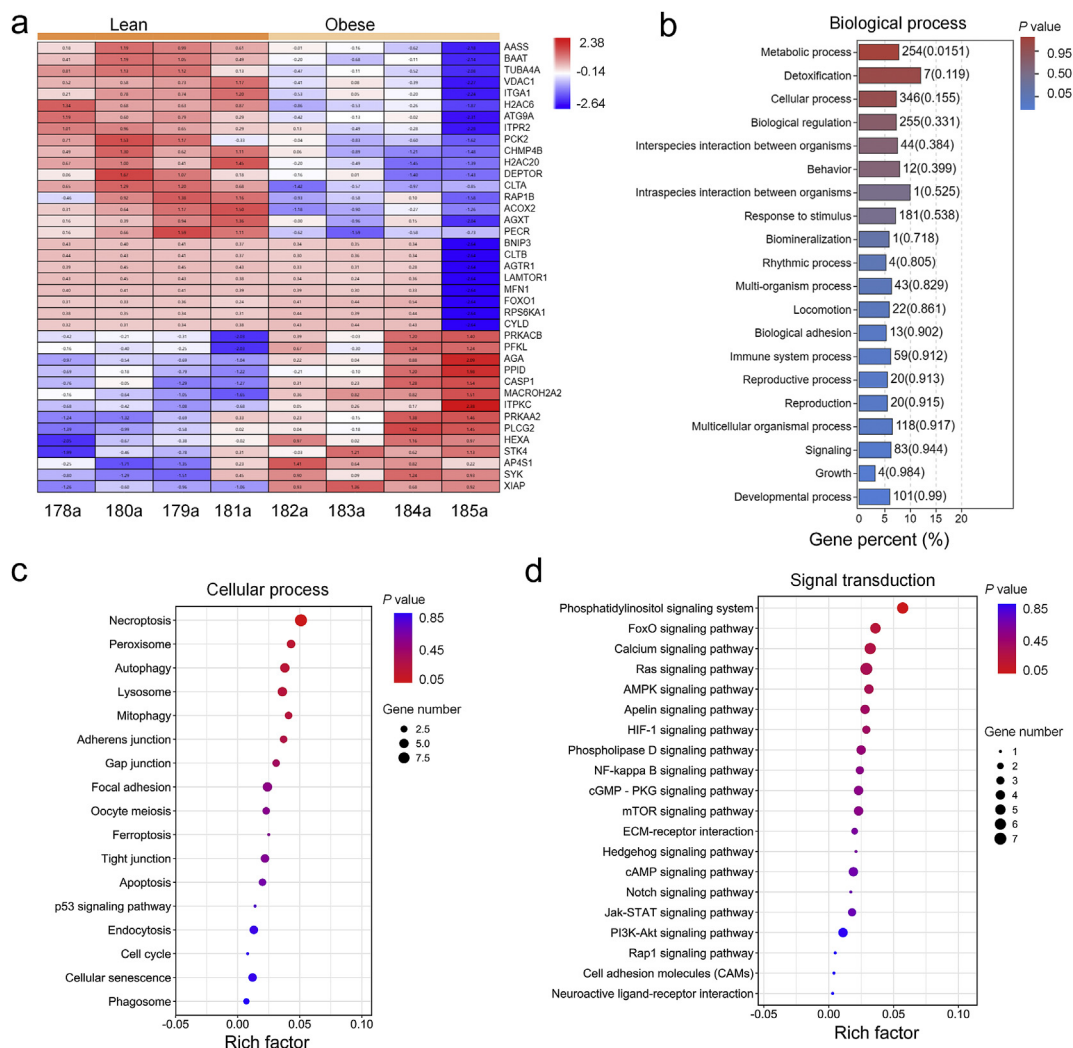


**Figure 2** Biological process, molecular events, and cell signaling pathways in livers from lean and obese human liver samples were analyzed using label-free quantitative proteomics and LC-MS/MS to identify differentially expressed proteins. (a) Heatmap displays significantly regulated proteins in signaling pathways of PI3K-Akt, AMPK, and FoxO, as well as cellular processes of autophagy and mitophagy. (b) GO analysis was conducted with all altered proteins, and 20 highest-ranking biological process terms are shown. (c) KEGG pathway analyses of all significantly regulated proteins were performed, and the enrichment for cellular process of KEGG pathway is shown using bubble plot. (d) Bubble plot displays the enrichment for signal transduction of KEGG pathway.

including *Scd-1*, gluconeogenesis including *Pepck* and *G6pase*, and triglycerides synthesis including *Dgat1* in WT groups. The effects were reconciled by DKO but not ablation of either *Akt2* or *AMPK $\alpha$ 2*. Removal of *Akt2*, *AMPK $\alpha$ 2*, or both, did not affect expression of these lipid metabolic genes under low fat diet intake condition (Fig. 6). This is supported by findings from Western blot analysis where high fat diet intake upregulated protein levels of FAS, CHREBP, SREBP1, PGC-1 $\alpha$ , PPAR $\alpha$ , PPAR $\gamma$ , SCD-1, GDAT1, PEPCK, and G6Pase in conjunction with decreased phosphorylation of fatty acid synthesis enzyme ACC (no change in pan-ACC) in WT groups. Ablation of *Akt2*, *AMPK $\alpha$ 2*, or both, failed to affect protein expression of these lipid metabolic enzymes under low fat diet intake condition (Fig. 7).

### 3.5. Changes in inflammation, autophagy, mitophagy, and autophagy signaling (*Akt*, *AMPK*, and *FoxO1*)

To determine the mechanisms behind DKO-offered protection against high fat diet-induced changes, body weight, hepatic injury,

levels of inflammatory, autophagy, mitophagy, and regulatory signaling were monitored in hepatic tissues from trial mice. Our data revealed that high fat diet intake significantly upregulated levels of the proinflammatory makers TNF- $\alpha$  and IL-6. Additionally, high fat diet intake decreased levels of autophagy and mitophagy marker LC3BII, Parkin, FUNDC1, and BNIP3 while elevating p62 and mitophagy marker TOM20 in WT mice. These effects, with the exception of FUNDC1 and BNIP3, were abolished in DKO but not *Akt2*<sup>-/-</sup> and *Ampk $\alpha$ 2*<sup>-/-</sup> mice (Fig. 8a-h). Moreover, high fat diet intake promoted phosphorylation of the autophagy regulatory signal FoxO1 without affecting pan protein level of FoxO1 in WT mice, the effects of which were nullified in DKO but not *Akt2*<sup>-/-</sup> and *Ampk $\alpha$ 2*<sup>-/-</sup> mice (Fig. 8i). Ablation of *Akt2*, *AMPK $\alpha$ 2*, or both, failed to display any effects on inflammation, autophagy, and mitophagy markers in the low fat diet setting (Fig. 8). Our further study revealed that high fat diet intake suppressed phosphorylation of AMPK at Thr<sup>172</sup>, the effect of which was not restored in DKO, *Akt2*<sup>-/-</sup>, or *Ampk $\alpha$ 2*<sup>-/-</sup> mice. *Ampk $\alpha$ 2*<sup>-/-</sup> and DKO mice both displayed reduced AMPK Thr<sup>172</sup>

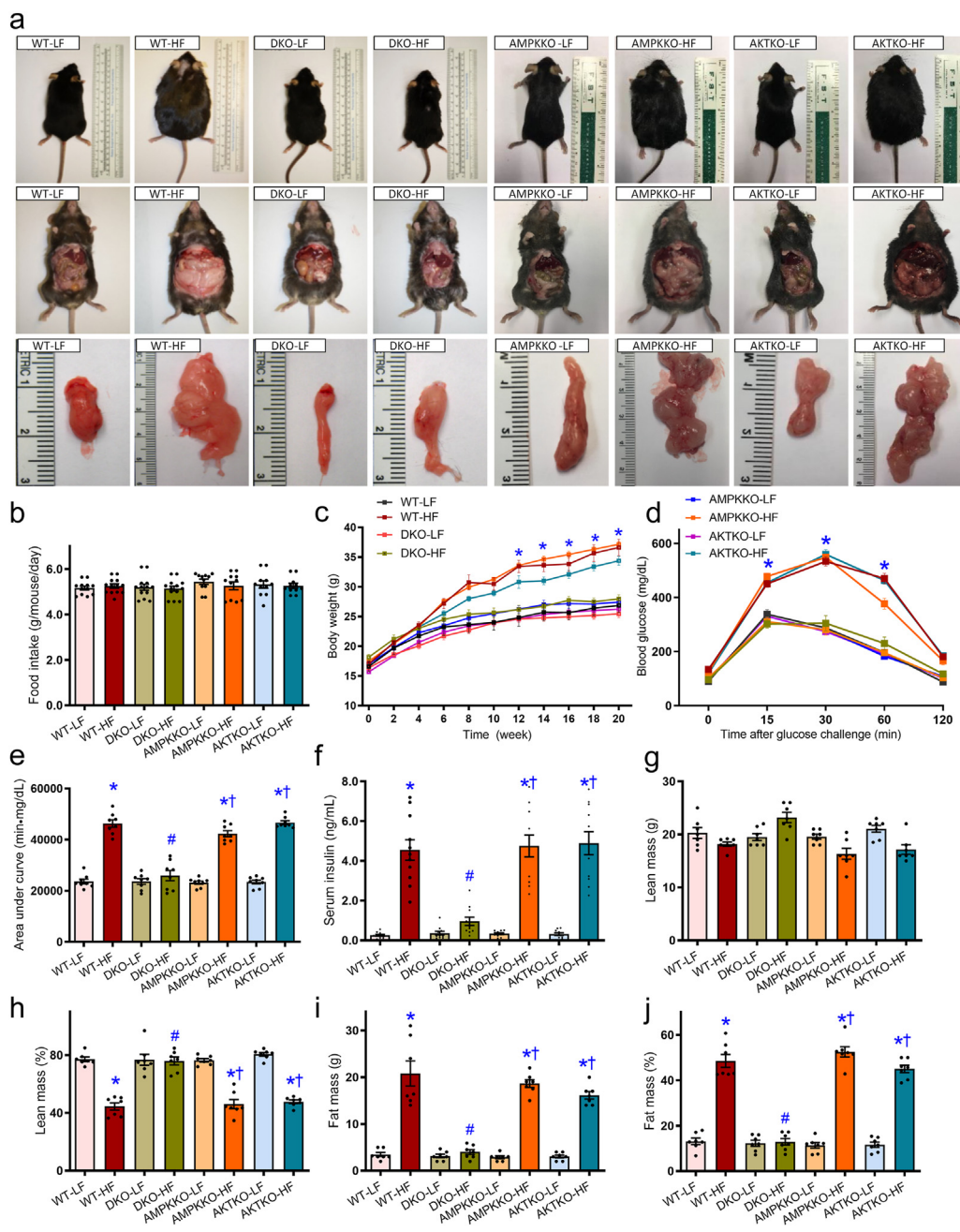


**Figure 3** Five week-old WT, *Ampkα2*<sup>-/-</sup>, *Akt2*<sup>-/-</sup>, and DKO mice were placed on a 45% high fat (HF) or nutritionally matched low fat (LF) diet for 20 weeks. (a) Representative photographs of mice (prone and supine positions) and white adipose tissues. (b) Food intake (per mouse daily,  $P > 0.05$ ). (c) Trajectory of body weight of WT and DKO mice. (d) Intraperitoneal glucose tolerance test (IPGTT). (e) Area under curve (AUC) for IPGTT. (f) Serum insulin level. (g) Lean mass weight. (h) Lean mass percentage. (i) Fat mass weight. (j) Fat mass percentage. Data are expressed as mean  $\pm$  SEM ( $n = 11-13$  for panels b–e,  $n = 7$  for panels f–j). \* $P < 0.05$  vs. WT mice; # $P < 0.05$  vs. WT-HF mice; † $P < 0.05$  vs. DKO-HF mice.

phosphorylation and pan-AMPK level (due to *Ampkα2* knockout) with low fat intake (Fig. 9a, d, and g). Meanwhile, high fat diet intake promoted phosphorylation of AMPK $\alpha$ 1 at Ser<sup>485</sup> (but not pan-AMPK $\alpha$ 1 protein) and Akt Ser<sup>473</sup> in WT mice (with exception of corresponding single ablation group), the effects of which were nullified in DKO and *Akt2*<sup>-/-</sup>, but not *Ampkα2*<sup>-/-</sup> mice (Fig. 9b, c, e, and f). Basal Akt phosphorylation was dampened in DKO and *Akt2*<sup>-/-</sup> mice receiving low fat diet (Fig. 9f). Deletion of Akt2, AMPK $\alpha$ 2, or both, explicitly decreased pan protein levels

of corresponding gene without affecting levels of the non-targeted protein including AMPK $\alpha$ 1 subunit (Fig. 9a–h and Supporting Information Fig. S1).

### 3.6. Role of autophagy and FoxO1 signaling in palmitic acid-induced lipid accumulation

To describe a possible role of autophagy and FoxO1 signaling in high fat diet-induced hepatic steatosis, HepG2 cells were

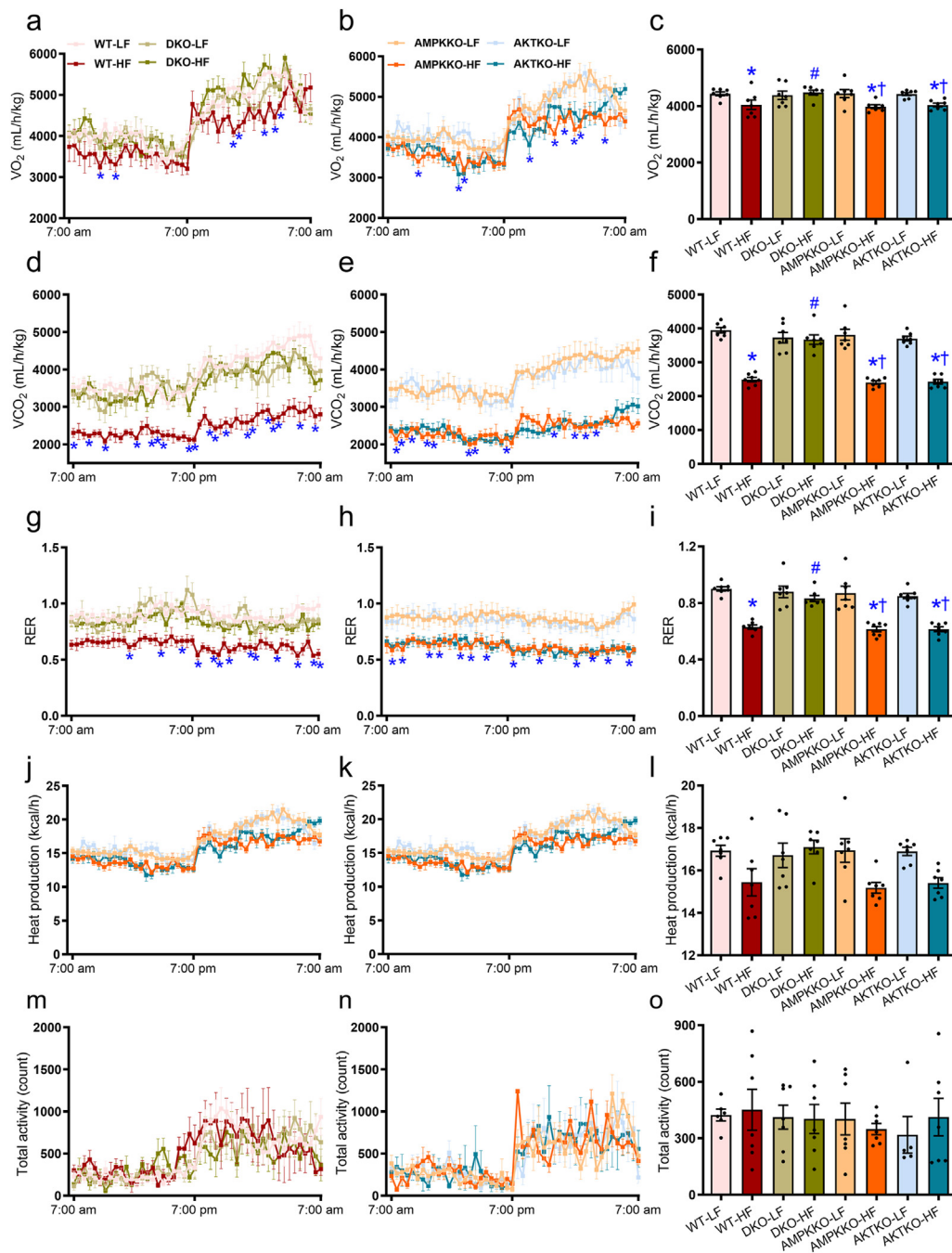


**Figure 4** Metabolic properties (24-h cycle) of WT, *Ampk2*<sup>-/-</sup>, *Akt2*<sup>-/-</sup>, and DKO mice fed LF or HF diet for 20 weeks. (a) O<sub>2</sub> consumption in DKO and WT groups. (b) O<sub>2</sub> consumption in *Ampk2*<sup>-/-</sup> and *Akt2*<sup>-/-</sup> mice. (c) Pooled data of O<sub>2</sub> consumption (24 h). (d) CO<sub>2</sub> production in DKO and WT mice. (e) CO<sub>2</sub> production in *Ampk2*<sup>-/-</sup> and *Akt2*<sup>-/-</sup> mice. (f) Pooled data of CO<sub>2</sub> production (24 h). (g) Respiratory exchange ratio (RER) in DKO and WT mice. (h) RER in *Ampk2*<sup>-/-</sup> and *Akt2*<sup>-/-</sup> mice. (i) Pooled data of RER (24 h). (j) Heat production in DKO and WT mice. (k) Heat production in *Ampk2*<sup>-/-</sup> and *Akt2*<sup>-/-</sup> mice. (l) Pooled data of heat production (24 h). (m) Total physical activity in DKO and WT mice. (n) Total physical activity in *Ampk2*<sup>-/-</sup> and *Akt2*<sup>-/-</sup> mice. (o) Pooled data of total physical activity (24 h). Data are expressed as mean ± SEM (*n* = 7). \**P* < 0.05 vs. WT mice; #*P* < 0.05 vs. WT-HF mice; †*P* < 0.05 vs. DKO-HF mice.

transfected with siRNA against *AKT2* and *AMPK* (or scramble RNA as control) prior to exposure to palmitic acid for 72 h in the presence or absence of the autophagy inhibitor 3-MA or the FoxO1 inhibitor AS1842856. Lipid accumulation was assessed using oil red O staining. Our data revealed that palmitic acid promoted lipid accumulation, the effect of which was negated by silencing *AKT2* and *AMPK* concurrently with little effect from

silencing *AKT2* and *AMPK* individually. Interestingly, both 3-MA and AS1842856 nullified *AKT2*–*AMPK* silencing-induced protection against palmitic acid-induced lipid accumulation without effect itself (Fig. 9i and j). This is consistent with the finding that 3-MA and AS1842856 removed *AKT2*–*AMPK* silencing-induced beneficial effect against palmitic acid-induced rise in cellular triglyceride levels (Fig. 9k).

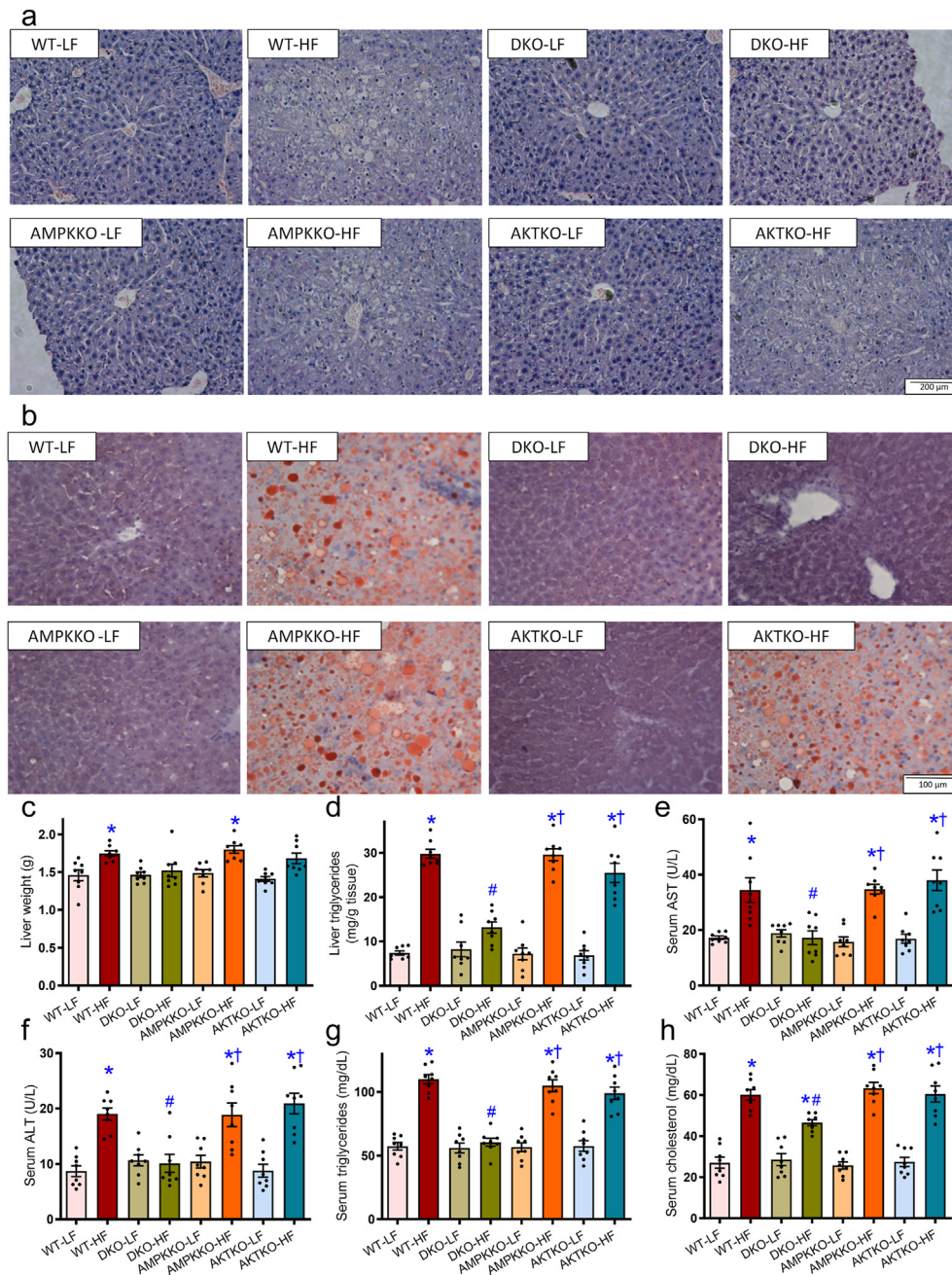


**Figure 5** Effects of *Ampk2*<sup>-/-</sup>, *Akt2*<sup>-/-</sup>, and DKO on NAFLD. (a) Hematoxylin and eosin (H&E) staining of liver cross-sections from mice fed LF or HF diet for 20 weeks. (b) Representative oil red O staining micrographs. (c) Liver weight. (d) Liver triglyceride content. (e) Serum AST levels. (f) Serum ALT levels. (g) Serum triglyceride levels. (h) Serum cholesterol levels. Data are expressed as mean  $\pm$  SEM ( $n = 8$ ). \* $P < 0.05$  vs. WT mice; # $P < 0.05$  vs. WT-HF mice; † $P < 0.05$  vs. DKO-HF mice.

### 3.7. Role of Parkin in DKO-offered benefit against high fat diet-induced obesity, adiposity, and hepatic steatosis

Given that Parkin is the only mitophagy marker correlated with DKO-induced beneficial effect against high fat intake, we went on to cross DKO mice with *Prk*<sup>-/-</sup> mice to generate a TKO model. Our data, shown in Fig. 10, revealed that high fat diet intake significantly increased body weight in WT mice starting from 12 weeks of diet feeding. However, this effect was spared in *Prk*<sup>-/-</sup> or TKO mice (Fig. 10a and b). In addition, high fat diet overtly increased white adipose tissues (inguinal, epididymal, and

retroperitoneal), brown adipose tissues, and spleen (but not kidney) weight in WT mice, the effect of which was not seen in *Prk*<sup>-/-</sup> or DKO mice (Fig. 10a and c–f). To evaluate the role of Parkin in fat diet intake- and DKO-induced hepatic steatosis, levels of triglycerides and cholesterol were evaluated. High fat intake promoted hepatomegaly, hepatic steatosis, liver triglyceride accumulation, and hyperlipidemia in WT mice although *Prk*<sup>-/-</sup> or TKO mice were unaffected. Ablation of Parkin or triple knockout did not display any effects on hepatic morphology, triglycerides, or serum profiles of lipid in the face of low fat diet intake (Supporting Information Fig. S3). These findings suggested that Parkin

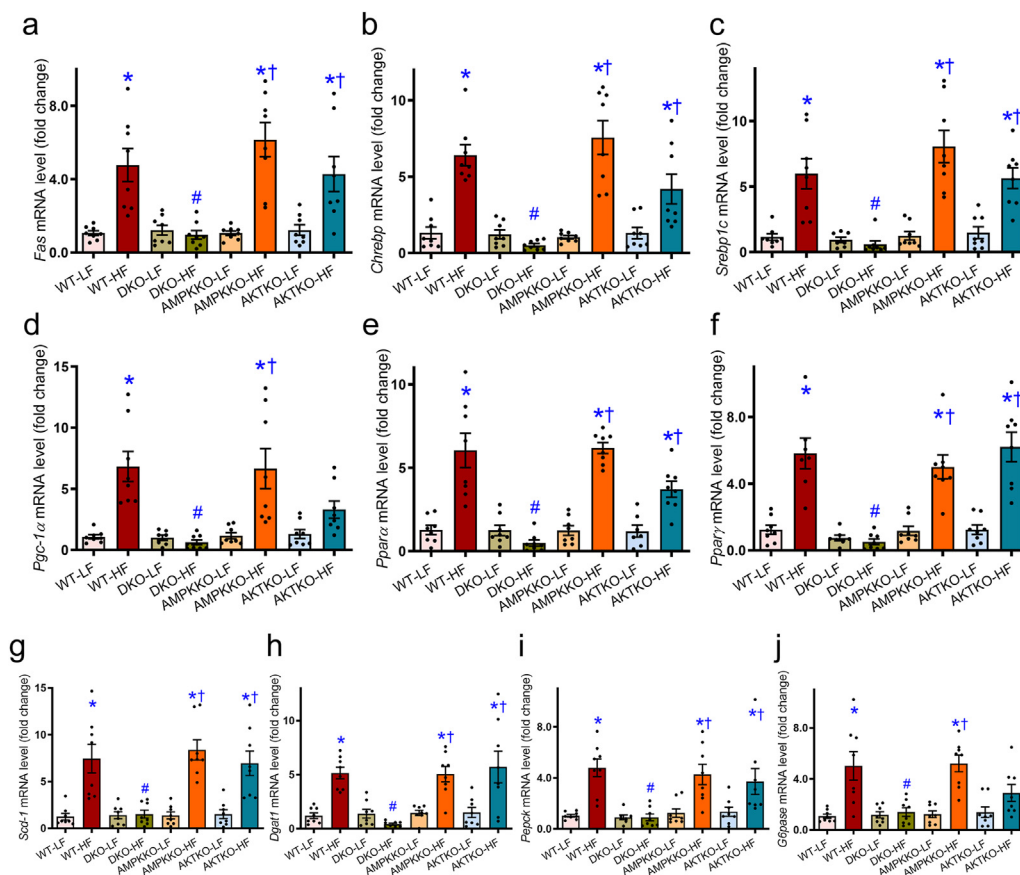


**Figure 6** Effect of *Ampkα2*<sup>-/-</sup>, *Akt2*<sup>-/-</sup>, and DKO on levels of lipid regulatory genes in livers from mice fed LF or HF diet using real time-PCR analysis. (a–j) The mRNA levels of *Fas* (a), *Chrebp* (b), *Srebp1c* (c), *Pgc-1α* (d), *Pparα* (e), *Pparγ* (f), *Scd-1* (g), *Dgat1* (h), *Pepck* (i), and *G6pase* (j) were examined. Data are expressed as mean ± SEM (*n* = 8–9). \**P* < 0.05 vs. WT mice; #*P* < 0.05 vs. WT-HF mice; †*P* < 0.05 vs. DKO-HF mice.

ablation removed the DKO-induced benefit on adiposity, hepatic steatosis, and dyslipidemia.

### 3.8. Role of Parkin in DKO-offered benefits against fat diet-induced hepatic lipid anomalies

To evaluate the impact of Parkin on DKO-induced benefit against high fat diet-induced hepatic lipid metabolic anomalies, lipid synthesis, uptake, and transport genes were evaluated using Western blot analysis. As depicted in Supporting Information Fig. S4, high fat diet intake clearly upregulated protein levels of FAS, CHREBP, SREBP1, PGC-1 $\alpha$ , PPAR $\alpha$ , PPAR $\gamma$ , SCD-1, DGAT1, PEPCCK, and G6Pase, as well as reduced ACC phosphorylation in WT mice. These effects were unaffected by *Prk*<sup>-/-</sup> or TKO. Parkin knockout or TKO did not display any effects on these lipid metabolic enzymes themselves under low fat diet intake.

### 3.9. Changes of Akt, AMPK, FoxO1, autophagy, and mitophagy in obese human livers

Levels of Akt, AMPK, FoxO1, autophagy, and mitophagy along with hepatic morphology were evaluated in liver specimens taken from lean and obese human subjects. Our data revealed microvesicular lipid accumulation and hepatocyte ballooning with rarefaction of hepatocyte cytoplasm along with hepatic steatosis

(oil red deposition) in obese human liver specimens (Fig. 11a). Similar to the rodent model of obesity, phosphorylation of Akt, AMPK (Ser<sup>485</sup>), and FoxO1 was elevated, while markers of autophagy and mitophagy (LC3B, Pink1, and Parkin) were downregulated in human obese livers (Fig. 11b–g).

## 4. Discussion

The salient findings from our study indicate that concurrent ablation of *Akt2* and *AMPKα2* protects against high fat diet intake-induced adiposity, hepatic steatosis, and liver injury. Our study revealed that high fat intake-induced hepatic steatosis is closely associated with suppressed mitophagy and activation of proinflammatory responses in the liver in the absence of altered food intake, energy expenditure, and physical activity. Double ablation of *Akt2* and *AMPKα2*, but not either alone, protected against high fat feeding-induced rises in mRNA and protein levels of enzymes governing lipogenesis (FAS, CHREBP, and SREBP1), lipid metabolism (PGC-1 $\alpha$  and PPAR $\alpha$ ), lipid storage (PPAR $\gamma$ ), unsaturated fatty acid synthesis (SCD-1), gluconeogenesis (PEPCK and G6Pase), and triglyceride synthesis (DGAT1). These changes in lipid metabolism were consistent with findings from serum and hepatic levels of triglycerides and cholesterol in single or DKO mice receiving low or high fat diet. Furthermore, double rather than single ablation of *Akt2* and *AMPKα2* protected against high fat diet-induced

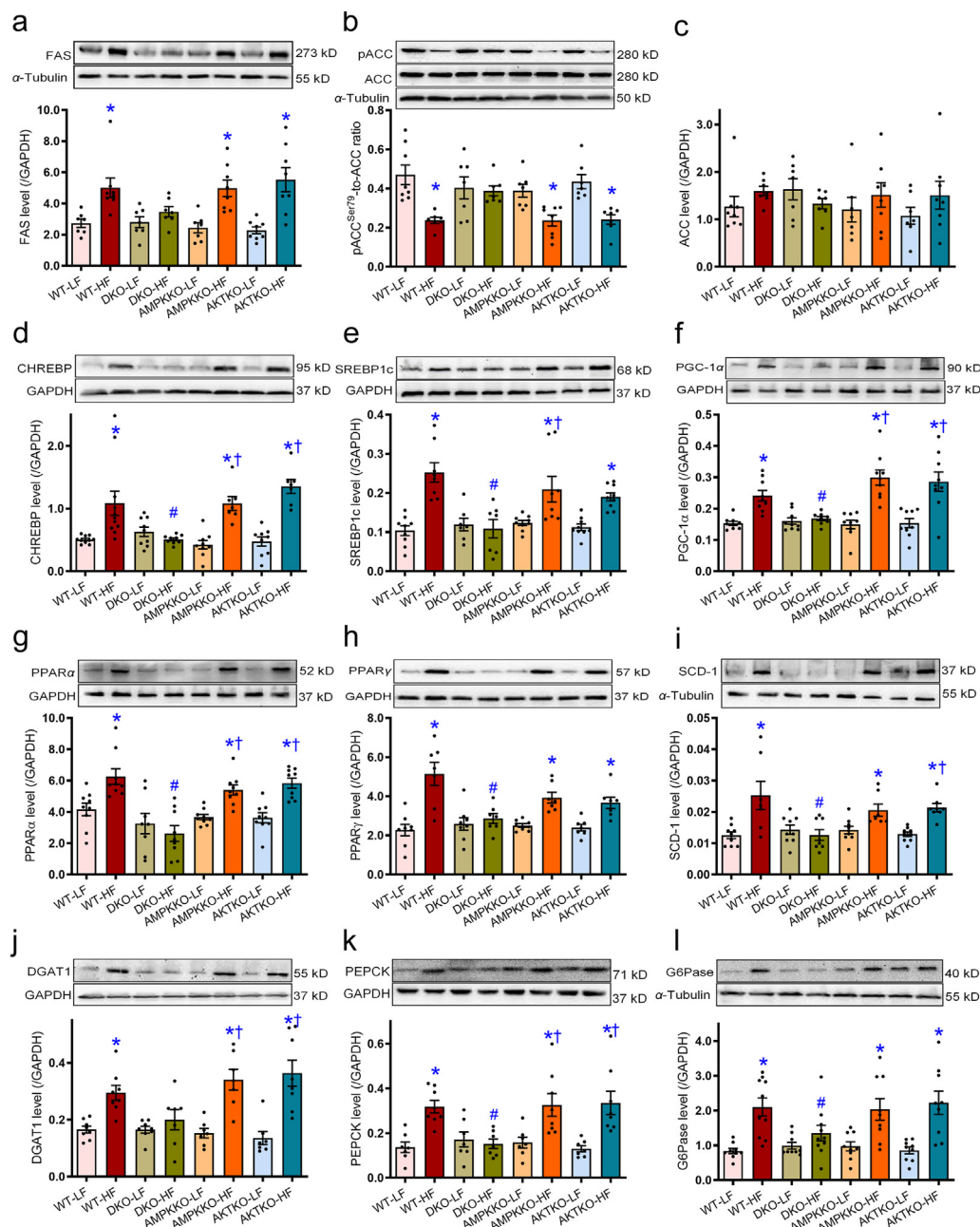


**Figure 7** Effects of *Ampka2*<sup>-/-</sup>, *Akt2*<sup>-/-</sup>, and DKO on the levels of lipid regulatory proteins in livers from mice fed LF or HF diet. (a–l) The protein levels of lipid synthesis, metabolism, and storage enzymes, including FAS (a), ACC (phosphorylated ACC and pan-ACC, pACC-to-ACC ratio, b), pan-ACC (c), CHREBP (d), SREBP1c (e), PGC-1 $\alpha$  (f), PPAR $\alpha$  (g), PPAR $\gamma$  (h), SCD-1 (i), DGAT1 (j), PEPCCK (k), and G6Pase (l), were examined using Western blot analysis. Representative gel blots which depicted the levels of lipid regulatory proteins (using GAPDH or  $\alpha$ -tubulin as loading control) were shown. Data are expressed as mean  $\pm$  SEM ( $n = 7$ –10). \* $P < 0.05$  vs. WT mice; # $P < 0.05$  vs. WT-HF mice; † $P < 0.05$  vs. DKO-HF mice.

phosphorylation (inactivation) of nuclear transcriptional factor FoxO1, an essential regulator for autophagy, glucose homeostasis, and lipid metabolism<sup>27,46</sup>. *In vitro* findings revealed that *AKT2*–*AMPK* co-silencing rescued against palmitic acid-induced lipid accumulation likely through an autophagy- and FoxO1-dependent mechanism. Data from obese human livers provided supporting evidence of overactivated Akt2, AMPK (Ser<sup>485</sup>), and FoxO1 along with compromised autophagy/mitophagy. RNAseq and mass spectrometry analyses from rodent

and human livers validated the GO terms (*e.g.*, lipid catabolic and fatty acid metabolic processes), KEGG pathways (*e.g.*, autophagy and mitophagy) and involvement of Akt, AMPK, and FoxO signaling as the most relevant enriched KEGG pathways in obese livers. Taken together, our current data demonstrated a beneficial role of concurrent ablation of *Akt2* and *AMPK $\alpha$ 2* against high fat diet intake-induced obesity, hepatic steatosis, and liver injury related to regulation of FoxO1-mediated autophagy/mitophagy and inflammation.

Hepatic injury due to a chronic high fat diet intake is likely caused by overconsumption of fatty acids, which interrupts hepatic ability for fat metabolism and storage. Triglycerides, the main form of fat to accommodate energy metabolism, accumulate within liver cells leading to steatosis, a hallmark of NAFLD. These features are consistent with the elevated serum ALT/AST, serum and hepatic cholesterol and triglycerides along with hepatic steatosis and hepatomegaly following high fat diet intake in our current experimental setting. Notably, results from our study indicated that high fat diet intake-induced hepatomegaly, hepatic steatosis, and liver injury were negated by *Akt2*–*Ampkα2* DKO (but not single knockout or TKO). These findings favor a beneficial role of *Akt2*–*Ampkα2* DKO in preserving hepatic homeostasis against high fat diet intake. Moreover, DKO of *Akt2*–*Ampkα2* protected against high fat diet-induced adiposity. Assessment of global metabolism using CLAMS did not favor a major contribution for altered food intake or energy expenditure in *Akt2*–*AMPKα2* double ablation. Heat production did not change

across experimental groups. RER, the ratio between CO<sub>2</sub> production and O<sub>2</sub> consumption, denotes the type of energetic substrate utilized. A RER value around 0.8 in low fat diet-fed mice usually indicates fatty acid oxidation and carbohydrate oxidation as the main energy source<sup>47</sup>. Our data revealed significantly lower RER (along with decreased O<sub>2</sub> consumption and CO<sub>2</sub> production) following high fat diet intake in WT, *Akt2*<sup>−/−</sup>, and *Ampkα2*<sup>−/−</sup> mice, denoting predominant usage of fat over carbohydrate for oxidation<sup>48</sup>. Intriguingly, *Akt2*–*Ampkα2* DKO reduced high fat diet intake-induced anomalies in global metabolism. *Akt2*–*AMPKα2* ablation favored utilization of carbohydrates as the main energy source. DKO also exerted positive effects on glucose tolerance tests and serum insulin levels, indicating preserved glucose metabolism. Perhaps the most interesting finding from our current study was DKO-offered protection against high fat diet-induced increases in mRNA and protein levels of enzymes governing lipid metabolism, the effect which vanished in the TKO model. DKO of *Akt2*–*Ampkα2* reversed high fat diet-induced rises

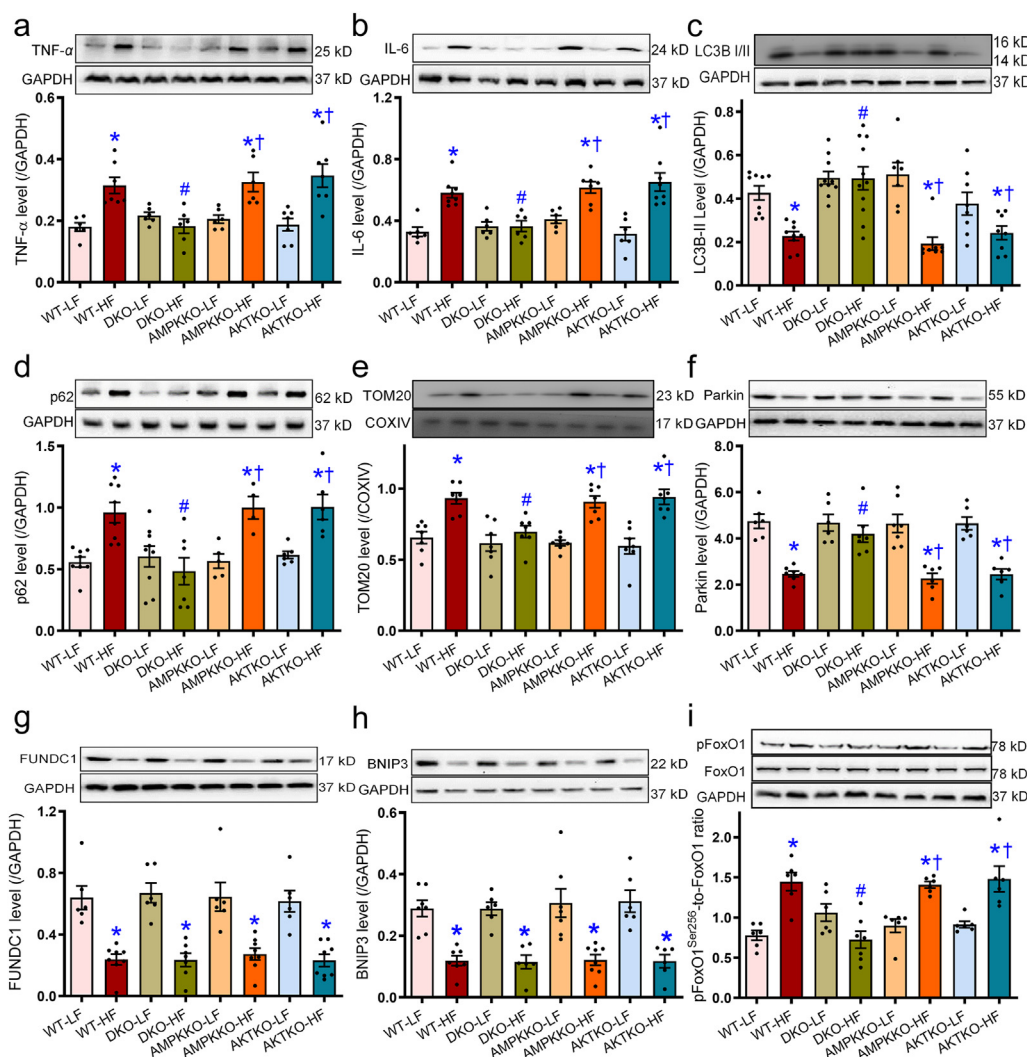


**Figure 8** Effects of *Ampkα2*<sup>−/−</sup>, *Akt2*<sup>−/−</sup>, and DKO on the levels of inflammatory cytokines, autophagy/mitophagy markers, and FoxO1 in livers from mice fed LF or HF diet. The protein levels of TNF-α (a), IL-6 (b), LC3BII (c), p62 (d), TOM20 (e), Parkin (f), FUNDC1 (g), BNIP3 (h), and FoxO1 (phosphorylated and pan-, pFoxO1-to-FoxO1 ratio, i) were examined using Western blot analysis. Representative gel blots which depicted the levels of TNF-α, IL-6, LC3BI/II, p62, TOM20, Parkin, FUNDC1, BNIP3, FoxO1, and phosphorylated FoxO1 were shown. Data are expressed as mean ± SEM ( $n = 6-9$ ). \* $P < 0.05$  vs. WT mice; # $P < 0.05$  vs. WT-HF mice; † $P < 0.05$  vs. DKO-HF mice.

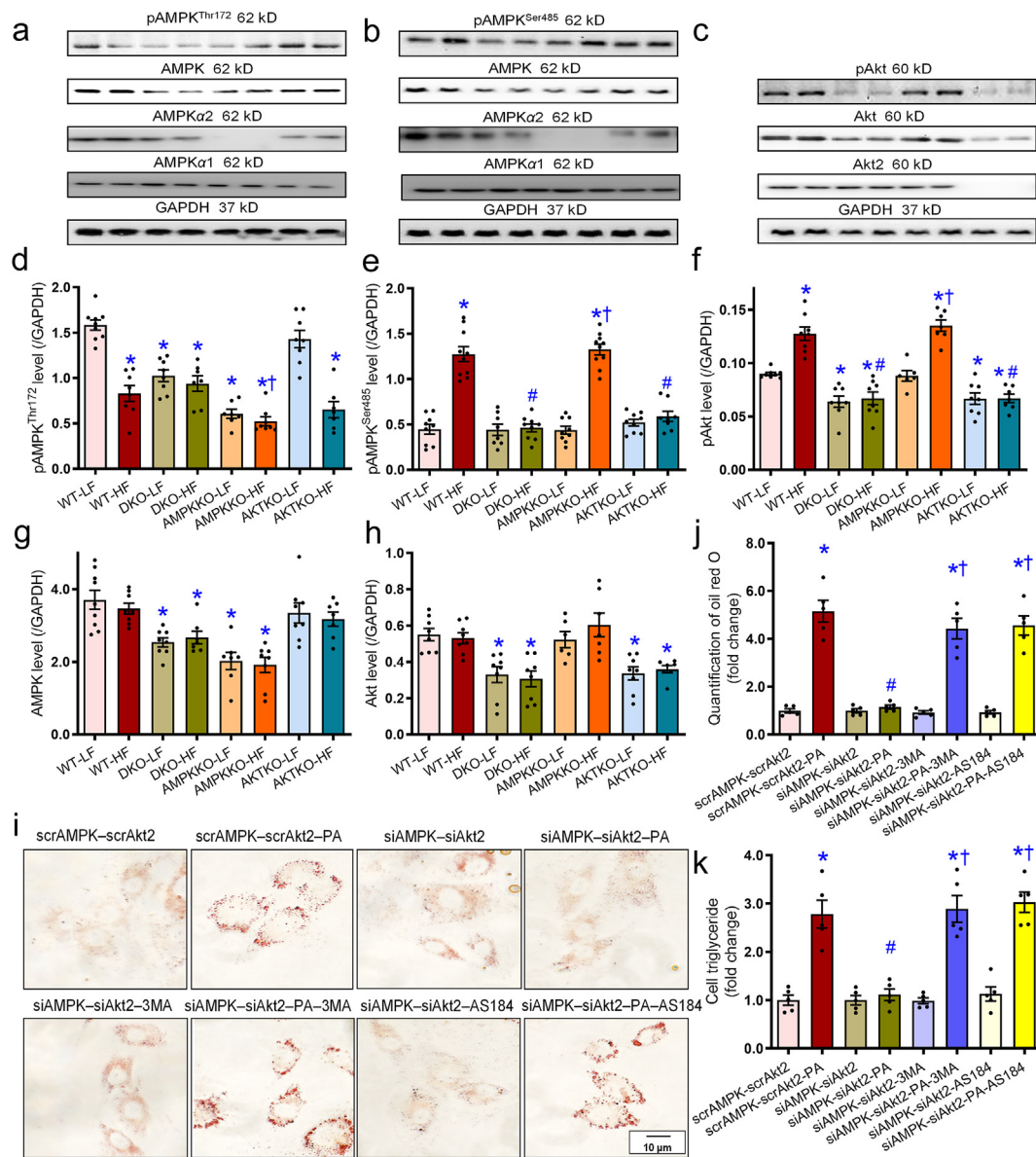


**Figure 9** Effect of *Ampkα2*<sup>-/-</sup>, *Akt2*<sup>-/-</sup>, and DKO on pan- and phosphorylated levels of AMPK and Akt in mice livers and the effects of *Ampk* and *Akt2* knockdown on palmitic acid (PA)-induced lipid accumulation in HepG2 cells. (a–c) Representative gel blots of panels d–h depicting pan- and phosphorylated AMPK and Akt as well as AMPK $\alpha$ 1, AMPK $\alpha$ 2, and Akt2 subunits using specific antibodies. (d) pAMPK (Th<sup>172</sup>)-to-GAPDH ratio. (e) pAMPK (Ser<sup>485</sup>)-to-GAPDH ratio. (f) pAkt (Ser<sup>473</sup>)-to-GAPDH ratio. (g) AMPK levels. (h) Akt level. (i–k) Cells were treated with scrAMPK-scrAkt2 or siAMPK-siAkt2 prior to exposure to PA (0.5 mmol/L) in the presence or absence of the autophagy inhibitor 3-MA (10 mmol/L) and the FoxO1 inhibitor AS1842856 (100 nmol/L) for 72 h. Representative oil red O staining images from the indicated HepG2 groups (i), quantification of oil red O (j), and cellular triglyceride levels (k) were shown. Data are expressed as mean  $\pm$  SEM ( $n = 7–9$  mice per group, panels a–h;  $n = 5$  independent experiments, panels j and k). \* $P < 0.05$  vs. WT mice or scrAMPK-scrAKT group; # $P < 0.05$  vs. WT-HF mice or scrAMPK-scrAKT-PA group; † $P < 0.05$  vs. DKO-HF mice or siAMPK-siAKT-PA group.

in lipid synthetic, metabolic and storage enzymes. These metabolic effects were absent in single knockout and TKO groups. The observations utilizing lipid enzyme profiles were supported by anthropometric, CLAMS metabolic data, glucose tolerance tests, and serum lipid profiles.

Our results further indicated that 5-month of chronic high fat intake suppressed hepatic autophagy, mitophagy, and promoted inflammation in WT mice. These effects were reconciled by *Akt2*–*Ampkα2* DKO but not *Akt2*<sup>-/-</sup> and *Ampkα2*<sup>-/-</sup> mice. These findings suggested potential contribution of mitophagy and

inflammation in DKO-elicited beneficial effects on hepatic steatosis and liver function in the face of high fat diet intake. This is supported by evidence from our lab and others, favoring an essential role for disturbed autophagy and promoted inflammation in genetic and diet-induced obesity, hepatic steatosis and liver injury<sup>8,10,27,33,35</sup>. Finally, ablation of Parkin nullified *Akt2*–*Ampkα2* DKO-induced protection against hepatic steatosis. Induction of mitophagy in particular Pink1–Parkin-dependent mitophagy was demonstrated to suppress lipid accumulation through downregulation of *de novo* lipogenesis genes including

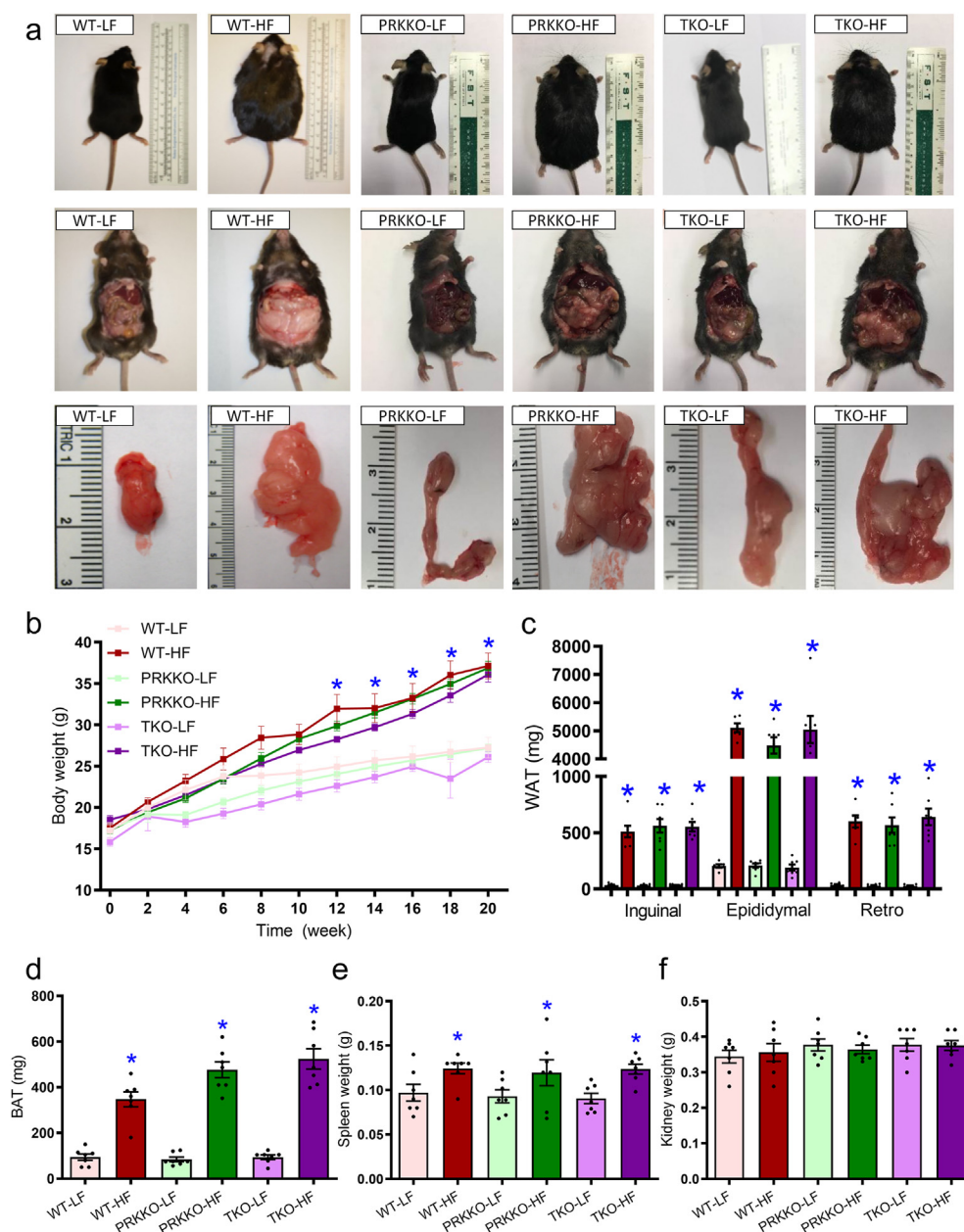


**Figure 10** Five week-old WT, *Prk*<sup>-/-</sup>, *Akt2*<sup>-/-</sup>–*Ampka2*<sup>-/-</sup>–*Prk*<sup>-/-</sup> triple knockout (TKO) mice were placed on a 45% HF or nutritionally matched LF diet for 20 weeks. (a) Representative photographs of mice (prone and supine positions) and white adipose tissues. (b) Trajectory of body weight of WT, *Prk*<sup>-/-</sup>, and TKO mice. (c) White adipose tissue (WAT). (d) Brown adipose tissue (BAT). (e) Spleen weight. (f) Kidney weight. Data are expressed as mean ± SEM (*n* = 7). \**P* < 0.05 vs. WT mice.

PPAR $\alpha$ , SREBP1c, FAS, and ACC in high fat diet challenged livers<sup>49,50</sup>. Although it is beyond the scope of current study, proinflammatory responses are likely an effector of disturbed autophagy in high fat diet-induced hepatic steatosis and liver injury<sup>27</sup>. Further examination of FoxO1, a nuclear transcriptional factor downstream of both Akt and AMPK<sup>51</sup>, suggested that *Akt2*–*Ampka2* DKO reduced high fat diet-induced FoxO1 phosphorylation (denoting inactivation), a response that was absent in either *Akt2*<sup>-/-</sup> or *Ampka2*<sup>-/-</sup> mice. Among various transcription factors regulating autophagy, FoxO is perhaps the most prominent one with its regulation governed by phosphorylation and thus nuclear exclusion for inactivation<sup>26,46,52</sup>. FoxO1 is capable of regulating mitochondrial  $\beta$ -oxidation through PPAR $\alpha$ -dependent

mechanism to govern a wide array of cellular processes, including glucose and lipid metabolism<sup>52</sup>. Earlier evidence depicted distinct stimulatory and inhibitory roles for AMPK and Akt on FoxO1 activity, respectively<sup>26</sup>, thus leading to disparate responses on glucose, lipid, and protein metabolism, as well as cell survival. These actions may underlie Akt- and AMPK-induced biological responses in obesogenesis, insulin sensitivity, and NAFLD. Several studies have depicted a role for Akt in controlling hepatic steatosis through an mTOR-dependent mechanism. Elevated Akt phosphorylation was noted in livers from NAFLD patients alongside with dysregulated autophagy<sup>53</sup>. Akt activation, particular *Akt2* was shown to foster hepatic steatosis through SREBP1c regulation, suggesting its therapeutic value in the management of

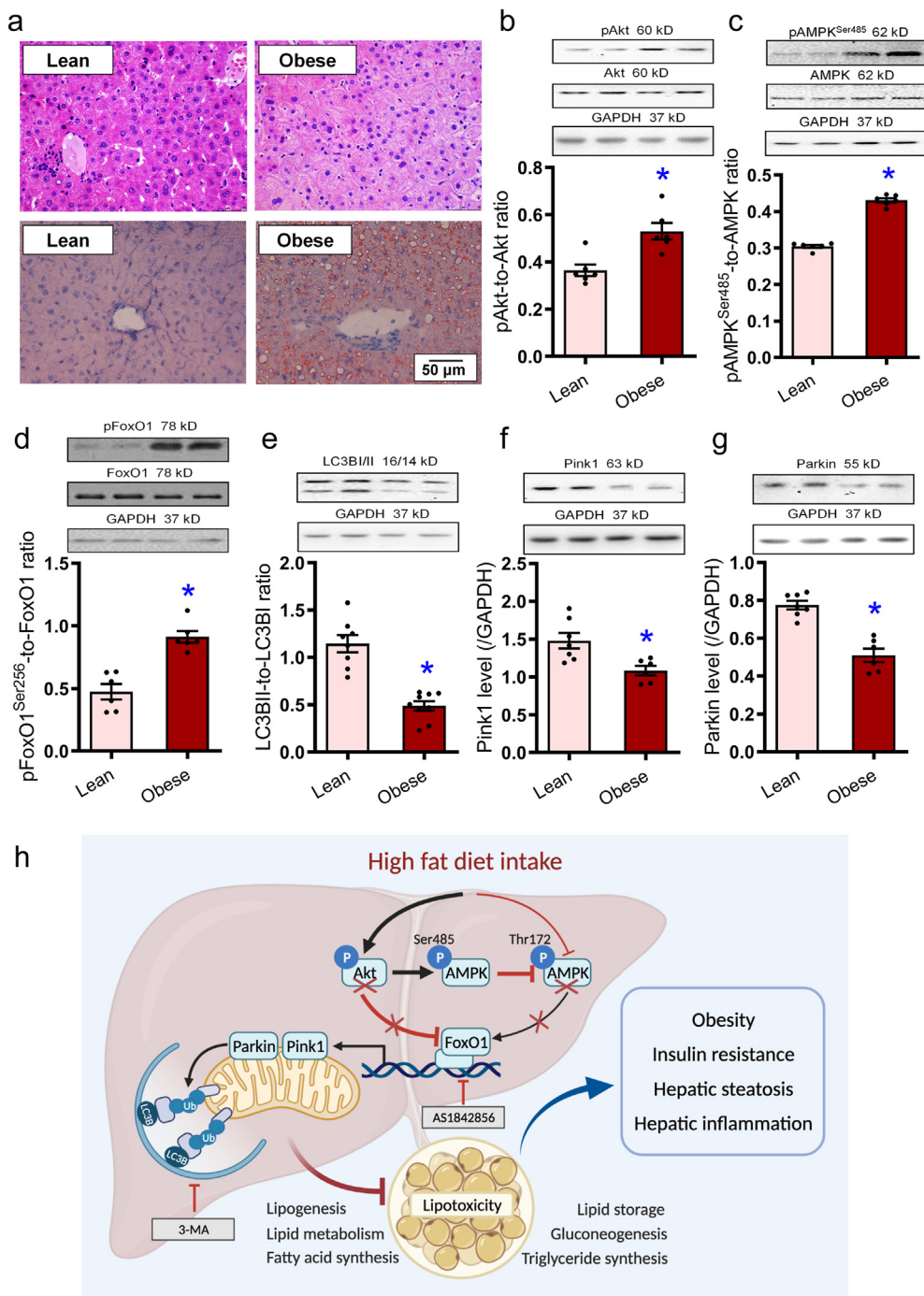


**Figure 11** Morphology, steatosis, cell signaling, autophagy, and Pink1–Parkin mitophagy in obese human liver specimen. (a) H&E staining of liver cross-sections and oil red O staining micrographs in lean and obese human liver samples. (b) pAkt-to-Akt ratio. (c) pAMPK (Ser<sup>485</sup>)-to-AMPK ratio. (d) pFoxO1<sup>Ser256</sup>-to-FoxO1 ratio. (e) LC3BII-to-LC3BI ratio. (f) Pink1. (g) Parkin. Representative gel blots depicting pan- and phosphorylated Akt, AMPK (Ser<sup>485</sup>), and FoxO1, as well as LC3BII/II, Pink1, and Parkin (GAPDH as loading controls) using specific antibodies were shown. Data are expressed as mean  $\pm$  SEM ( $n = 6-7$ ). \* $P < 0.05$  vs. lean group. h: Scheme depicting possible mechanism(s) for the role of Akt2, AMPK, and Parkin-mediated mitophagy in high fat diet-induced obesity and hepatic steatosis. Chronic high fat diet intake suppresses FoxO1-mediated mitophagy through parallel regulation of Akt and AMPK. On one hand, high fat intake promotes Akt phosphorylation leading to inhibition of FoxO1 (phosphorylation) and suppressed autophagy. On the other hand, high fat intake suppressed AMPK phosphorylation at Thr<sup>172</sup> and inhibition of autophagy. Hyperactivated Akt (phosphorylation) fosters AMPK phosphorylation at Ser<sup>485</sup>, disturbing AMPK phosphorylation at Thr<sup>172</sup> indirectly. Compromised FoxO1 signaling contributes to compromised lipid metabolism and lipid accumulation due to poor mitophagy, resulting in obesity, hepatic steatosis. Arrowheads denote stimulation whereas the lines with a “T” ending represent inhibition.

NAFLD<sup>23,54</sup>. Yecies and colleagues<sup>22</sup> revealed that Akt stimulated hepatic SREBP1c and lipogenesis *via* parallel mTOR-dependent and -independent pathways. These findings noted that mTORC1-independent pathway involves Akt-mediated decrease in the liver-specific transcript encoding the SREBP1c inhibitor INSIG2<sup>22</sup>. Data from our current study suggested that Akt2-promoted hepatic steatosis and liver injury in the face of high fat diet intake also required the “presence” of AMPK. Earlier reports supported a role for AMPK in Akt2-mediated hepatic lipid accumulation using ACC as the AMPK target<sup>23</sup>. AMPK is an essential cell fuel molecule with therapeutic benefit against high fat diet-induced hepatic steatosis and NAFLD<sup>55</sup>. Early findings from our lab showed worsened cardiac geometry and function with AMPK deficiency in the face of chronic high fat diet intake, without notable changes in global metabolism<sup>32</sup>. Our data revealed that *Akt2–Ampkα2* DKO nullified high fat diet-induced activation of Akt and AMPKα1 subunit (Ser<sup>485</sup>). Our results did not favor a “compensatory” role for AMPKα1 in the face of AMPKα2 ablation. Early evidence noted compromised AMPKα2 signaling but not that of AMPKα1 in livers following high fat diet intake<sup>56</sup>, in line with our current finding. Phosphorylation of AMPKα1 Ser<sup>485</sup> occurs downstream of Akt, to inhibit AMPK Thr<sup>172</sup> phosphorylation. As depicted in Fig. 11h, high fat diet intake may promote FoxO1 phosphorylation and autophagy/mitophagy inhibition *via* parallel hyperphosphorylation of Akt and dephosphorylation of AMPK. These findings are in line with stimulatory and inhibitory effects of autophagy, for AMPK and Akt, respectively<sup>26,57</sup>. In our hands, *Akt2–AMPKα2* double ablation was unable to restore fat diet-induced dephosphorylation of AMPK Thr<sup>172</sup> (possibly due to AMPKα2 ablation). Instead DKO abrogated Akt-induced suppression of FoxO1 and autophagy under high fat diet intake, an effect which was absent in *Akt2*<sup>−/−</sup> model. In addition, DKO of *Akt2–Ampkα2* removed Akt-induced AMPKα1 Ser<sup>485</sup> phosphorylation to improve “residual” AMPK Thr<sup>172</sup> phosphorylation<sup>58,59</sup> in the face of high fat diet intake. It is plausible to speculate that FoxO1 and Parkin mitophagy may serve as common converging points for Akt2 and AMPK signaling in high fat diet-induced obesity and hepatic steatosis.

Autophagy/mitophagy is essential for lipid droplet breakdown while defective autophagy perturbs lipid turnover and promotes lipid accumulation and fat storage<sup>60,61</sup>. It is noteworthy that unchecked autophagy was also reported in response to lipid overload, such as excess cholesterol or fatty acids<sup>62,63</sup>, as a compensatory defense mechanism to remove excess lipids<sup>27</sup>. Restored hepatic autophagy and mitophagy in *Akt2–Ampkα2* DKO mice noted in our study should help to remove excessive lipid droplets and preserve liver function. It should be mentioned that intrahepatic synthesis of triglycerides may function as an adaptive response to counter toxicity of triglyceride metabolites in high energy challenged models and obese individuals<sup>64,65</sup>. FoxO1 and mitophagy in DKO mice offered protection against high fat diet-induced hepatic steatosis and received consolidation from an *in vivo* study where Parkin ablation nullified *Akt2–AMPKα2* ablation-induced benefit. Additionally, our *in vitro* finding noted that inhibition of FoxO1 or autophagy abrogated *Akt2–Ampkα2* knockdown-induced benefit against palmitic acid-induced lipid accumulation. Given that uncorrected obesity serves as the main contributing factor for disturbed autophagy and lipid metabolism, hepatomegaly and liver injury<sup>8,27</sup>, it is possible that *Akt2–AMPKα2* double ablation-induced beneficial hepatic responses against high fat diet intake is secondary to DKO-induced

resistance of high fat diet-induced obesity. Last but not least, data from obese human livers supported the findings from mice. Further study is warranted to elucidate the direct hepatic response of Pink1–Parkin on lipid spillover and adiposity in the face of high fat diet intake.

## 5. Conclusions

Data from our study offers evidence that double ablation of Akt2 and AMPKα2 protects against high fat diet-induced obesity, hepatic steatosis and liver injury. Our study consolidated the notion of disturbed autophagy and augmented inflammation in hepatic steatosis and injury following high fat diet intake. More importantly, our findings favored that *Akt2–Ampkα2* DKO protects against hepatic steatosis, liver injury, and inflammation using FoxO1 and Parkin as the converging points. These findings should help explain the etiology of NAFLD in high fat diet-induced obesity and more importantly, the unique parallel regulation (and interaction) between Akt2 and AMPKα2 in global metabolism, glucose, and lipid metabolism, as well as hepatic homeostasis. These findings suggest the therapeutic promises of targeting Akt2 and AMPKα2 for drug development in the management of NAFLD and obesity.

## Acknowledgments

The authors greatly appreciate the assistance of Prof. Xiaowu Huang at Zhongshan Hospital Fudan University for collection of human liver specimens (Shanghai, China). Editorial assistance from Dr. Laurie J. Demillard from University of Wyoming School of Pharmacy (Laramie, WY, USA) is greatly appreciated. The work was supported in part by the National Key R&D Program of China (2017YFA0506000) and National Natural Science Foundation of China (82000351).

## Author contributions

Shuyi Wang, Jun Tao, Huaguo Chen, and Mechender Kandadi designed the experiments and analyzed data. Mingming Sun, Haixia Xu, and Yan Lu helped data collection. Gary Lopaschuk, Junmeng Zheng, and Hu Peng participated in study design and manuscript revision. Jun Ren was responsible for supervision and manuscript writing.

## Conflicts of interest

The authors declare no conflicts of interest.

## Appendix A. Supporting information

Supporting data to this article can be found online at <https://doi.org/10.1016/j.apsb.2021.07.006>.

## References

- Samuel VT, Shulman GI. Nonalcoholic fatty liver disease as a nexus of metabolic and hepatic diseases. *Cell Metabol* 2018;**27**:22–41.
- Trepo E, Valenti L. Update on NAFLD genetics: from new variants to the clinic. *J Hepatol* 2020;**72**:1196–209.
- Younossi ZM. Non-alcoholic fatty liver disease - a global public health perspective. *J Hepatol* 2019;**70**:531–44.

4. Eslam M, Newsome PN, Sarin SK, Anstee QM, Targher G, Romero-Gomez M, et al. A new definition for metabolic dysfunction-associated fatty liver disease: an international expert consensus statement. *J Hepatol* 2020;**73**:202–9.
5. Musso G, Cassader M, Gambino R. Non-alcoholic steatohepatitis: emerging molecular targets and therapeutic strategies. *Nat Rev Drug Discov* 2016;**15**:249–74.
6. Khan RS, Newsome PN. NAFLD in 2017: novel insights into mechanisms of disease progression. *Nat Rev Gastroenterol Hepatol* 2018;**15**:71–2.
7. Arguello G, Balboa E, Arrese M, Zanlungo S. Recent insights on the role of cholesterol in non-alcoholic fatty liver disease. *Biochim Biophys Acta* 2015;**1852**:1765–78.
8. Madrigal-Matute J, Cuervo AM. Regulation of liver metabolism by autophagy. *Gastroenterology* 2016;**150**:328–39.
9. Wang L, Chen J, Ning C, Lei D, Ren J. Endoplasmic reticulum stress related molecular mechanisms in nonalcoholic fatty liver disease (NAFLD). *Curr Drug Targets* 2018;**19**:1087–94.
10. Ueno T, Komatsu M. Autophagy in the liver: functions in health and disease. *Nat Rev Gastroenterol Hepatol* 2017;**14**:170–84.
11. Friedman SL, Neuschwander-Tetri BA, Rinella M, Sanyal AJ. Mechanisms of NAFLD development and therapeutic strategies. *Nat Med* 2018;**24**:908–22.
12. Tomic D, Kemp WW, Roberts SK. Nonalcoholic fatty liver disease: current concepts, epidemiology and management strategies. *Eur J Gastroenterol Hepatol* 2018;**30**:1103–15.
13. Listenberger LL, Han X, Lewis SE, Cases S, Farese Jr RV, Ory DS, et al. Triglyceride accumulation protects against fatty acid-induced lipotoxicity. *Proc Natl Acad Sci U S A* 2003;**100**:3077–82.
14. Mi Y, Tan D, He Y, Zhou X, Zhou Q, Ji S. Melatonin modulates lipid metabolism in HepG2 cells cultured in high concentrations of oleic acid: AMPK pathway activation may play an important role. *Cell Biochem Biophys* 2018;**76**:463–70.
15. Mendez-Sanchez N, Cruz-Ramon VC, Ramirez-Perez OL, Hwang JP, Barranco-Fragoso B, Cordova-Gallardo J. New aspects of lipotoxicity in nonalcoholic steatohepatitis. *Int J Mol Sci* 2018;**19**:2034.
16. Vatner DF, Majumdar SK, Kumashiro N, Petersen MC, Rahimi Y, Gattu AK, et al. Insulin-independent regulation of hepatic triglyceride synthesis by fatty acids. *Proc Natl Acad Sci U S A* 2015;**112**:1143–8.
17. Zhang Y, Whaley-Connell AT, Sowers JR, Ren J. Autophagy as an emerging target in cardiorenal metabolic disease: from pathophysiology to management. *Pharmacol Ther* 2018;**191**:1–22.
18. Park SS, Lee YJ, Song S, Kim B, Kang H, Oh S, et al. Lactobacillus acidophilus NS1 attenuates diet-induced obesity and fatty liver. *J Endocrinol* 2018;**237**:87–100.
19. Kim B, Figueroa-Romero C, Pacut C, Backus C, Feldman EL. Insulin resistance prevents AMPK-induced Tau dephosphorylation through Akt-mediated increase in AMPKSer-485 phosphorylation. *J Biol Chem* 2015;**290**:19146–57.
20. Kurauti MA, Costa-Junior JM, Ferreira SM, Dos Santos GJ, Protzek AO, Nardelli TR, et al. Acute exercise restores insulin clearance in diet-induced obese mice. *J Endocrinol* 2016;**229**:221–32.
21. Shiwa M, Yoneda M, Okubo H, Ohno H, Kobuke K, Monzen Y, et al. Distinct time course of the decrease in hepatic AMP-activated protein kinase and Akt phosphorylation in mice fed a high fat diet. *PLoS One* 2015;**10**:e0135554.
22. Yecies JL, Zhang HH, Menon S, Liu S, Yecies D, Lipovsky AI, et al. Akt stimulates hepatic SREBP1c and lipogenesis through parallel mTORC1-dependent and independent pathways. *Cell Metabol* 2011;**14**:21–32.
23. Leavens KF, Easton RM, Shulman GI, Previs SF, Birnbaum MJ. Akt2 is required for hepatic lipid accumulation in models of insulin resistance. *Cell Metabol* 2009;**10**:405–18.
24. Li Y, Xu S, Mihaylova MM, Zheng B, Hou X, Jiang B, et al. AMPK phosphorylates and inhibits SREBP activity to attenuate hepatic steatosis and atherosclerosis in diet-induced insulin-resistant mice. *Cell Metabol* 2011;**13**:376–88.
25. Xu X, Hua Y, Nair S, Zhang Y, Ren J. Akt2 knockout preserves cardiac function in high-fat diet-induced obesity by rescuing cardiac autophagosome maturation. *J Mol Cell Biol* 2013;**5**:61–3.
26. Zhao Y, Hu X, Liu Y, Dong S, Wen Z, He W, et al. ROS signaling under metabolic stress: cross-talk between AMPK and AKT pathway. *Mol Cancer* 2017;**16**:79.
27. Ge S, Xia X, Ding C, Zhen B, Zhou Q, Feng J, et al. A proteomic landscape of diffuse-type gastric cancer. *Nat Commun* 2018;**9**:1012.
28. Shi B, Ma M, Zheng Y, Pan Y, Lin X. mTOR and Beclin1: two key autophagy-related molecules and their roles in myocardial ischemia/reperfusion injury. *J Cell Physiol* 2019;**234**:12562–8.
29. Ren J, Sun M, Zhou H, Ajoolabady A, Zhou Y, Tao J, et al. FUNDC1 interacts with FBXL2 to govern mitochondrial integrity and cardiac function through an IP3R3-dependent manner in obesity. *Sci Adv* 2020;**6**:eabc8561.
30. Viollet B, Andreelli F, Jorgensen SB, Perrin C, Geloan A, Flamez D, et al. The AMP-activated protein kinase  $\alpha$ 2 catalytic subunit controls whole-body insulin sensitivity. *J Clin Invest* 2003;**111**:91–8.
31. Cho H, Mu J, Kim JK, Thorvaldsen JL, Chu Q, Crenshaw 3rd EB, et al. Insulin resistance and a diabetes mellitus-like syndrome in mice lacking the protein kinase Akt2 (PKB  $\beta$ ). *Science* 2001;**292**:1728–31.
32. Turdi S, Kandadi MR, Zhao J, Huff AF, Du M, Ren J. Deficiency in AMP-activated protein kinase exaggerates high fat diet-induced cardiac hypertrophy and contractile dysfunction. *J Mol Cell Cardiol* 2011;**50**:712–22.
33. Guo R, Nair S, Zhang Y, Ren J. Adiponectin deficiency rescues high-fat diet-induced hepatic injury, apoptosis and autophagy loss despite persistent steatosis. *Int J Obes (Lond)* 2017;**41**:1403–12.
34. Zhang Y, Babcock SA, Hu N, Maris JR, Wang H, Ren J. Mitochondrial aldehyde dehydrogenase (ALDH2) protects against streptozotocin-induced diabetic cardiomyopathy: role of GSK3 $\beta$  and mitochondrial function. *BMC Med* 2012;**10**:40.
35. Guo R, Xu X, Babcock SA, Zhang Y, Ren J. Aldehyde dehydrogenase-2 plays a beneficial role in ameliorating chronic alcohol-induced hepatic steatosis and inflammation through regulation of autophagy. *J Hepatol* 2015;**62**:647–56.
36. Kandadi MR, Hua Y, Zhu M, Turdi S, Nathanielsz PW, Ford SP, et al. Influence of gestational overfeeding on myocardial proinflammatory mediators in fetal sheep heart. *J Nutr Biochem* 2013;**24**:1982–90.
37. Wang Q, Ren J. mTOR-Independent autophagy inducer trehalose rescues against insulin resistance-induced myocardial contractile anomalies: role of p38 MAPK and Foxo1. *Pharmacol Res* 2016;**111**:357–73.
38. Yang X, Xu P, Zhang F, Zhang L, Zheng Y, Hu M, et al. AMPK hyperactivation alters fatty acids metabolism and impairs invasiveness of trophoblasts in preeclampsia. *Cell Physiol Biochem* 2018;**49**:578–94.
39. Vergadi E, Vaporidi K, Theodorakis EE, Doxaki C, Lagoudaki E, Ieronymaki E, et al. Akt2 deficiency protects from acute lung injury via alternative macrophage activation and miR-146a induction in mice. *J Immunol* 2014;**192**:394–406.
40. Zhang J, Fan N, Peng Y. Heat shock protein 70 promotes lipogenesis in HepG2 cells. *Lipids Health Dis* 2018;**17**:73.
41. Guo R, Hu N, Kandadi MR, Ren J. Facilitated ethanol metabolism promotes cardiomyocyte contractile dysfunction through autophagy in murine hearts. *Autophagy* 2012;**8**:593–608.
42. Truong TH, Dwyer AR, Diep CH, Hu H, Hagen KM, Lange CA. Phosphorylated progesterone receptor isoforms mediate opposing stem cell and proliferative breast cancer cell fates. *Endocrinology* 2019;**160**:430–46.
43. Zhu X, Yan H, Xia M, Chang X, Xu X, Wang L, et al. Metformin attenuates triglyceride accumulation in HepG2 cells through decreasing stearyl-coenzyme A desaturase 1 expression. *Lipids Health Dis* 2018;**17**:114.
44. Li R, Li J, Huang Y, Li H, Yan S, Lin J, et al. Polydatin attenuates diet-induced nonalcoholic steatohepatitis and fibrosis in mice. *Int J Biol Sci* 2018;**14**:1411–25.
45. Meng SX, Liu Q, Tang YJ, Wang WJ, Zheng QS, Tian HJ, et al. A recipe composed of Chinese herbal active components regulates hepatic lipid metabolism of NAFLD *in vivo* and *in vitro*. *Biomed Res Int* 2016;**2016**:1026852.

46. Tikhanovich I, Cox J, Weinman SA. Forkhead box class O transcription factors in liver function and disease. *J Gastroenterol Hepatol* 2013;**28** Suppl 1:125–31.
47. Oosterman JE, Foppen E, van der Spek R, Fliers E, Kalsbeek A, la Fleur SE. Timing of fat and liquid sugar intake alters substrate oxidation and food efficiency in male Wistar rats. *Chronobiol Int* 2015;**32**:289–98.
48. Ferrannini E. The theoretical bases of indirect calorimetry: a review. *Metabolism* 1988;**37**:287–301.
49. Liu P, Lin H, Xu Y, Zhou F, Wang J, Liu J, et al. Frataxin-mediated PINK1–Parkin-dependent mitophagy in hepatic steatosis: the protective effects of quercetin. *Mol Nutr Food Res* 2018;**62**:e1800164.
50. Wang L, Liu X, Nie J, Zhang J, Kimball SR, Zhang H, et al. ALCAT1 controls mitochondrial etiology of fatty liver diseases, linking defective mitophagy to steatosis. *Hepatology* 2015;**61**:486–96.
51. Sepa-Kishi DM, Katsnelson G, Bikopoulos G, Iqbal A, Ceddia RB. Cold acclimation reduces hepatic protein kinase B and AMP-activated protein kinase phosphorylation and increases gluconeogenesis in rats. *Phys Rep* 2018;**6**:e13592.
52. Xing YQ, Li A, Yang Y, Li XX, Zhang LN, Guo HC. The regulation of FOXO1 and its role in disease progression. *Life Sci* 2018;**193**:124–31.
53. Pang L, Liu K, Liu D, Lv F, Zang Y, Xie F, et al. Differential effects of reticulophagy and mitophagy on nonalcoholic fatty liver disease. *Cell Death Dis* 2018;**9**:90.
54. Zhang M, Chi X, Qu N, Wang C. Long noncoding RNA IncARSR promotes hepatic lipogenesis via Akt/SREBP-1c pathway and contributes to the pathogenesis of nonalcoholic steatohepatitis. *Biochem Biophys Res Commun* 2018;**499**:66–70.
55. Ou-Yang Q, Xuan CX, Wang X, Luo HQ, Liu JE, Wang LL, et al. 3-Acetyl-oleanolic acid ameliorates non-alcoholic fatty liver disease in high fat diet-treated rats by activating AMPK-related pathways. *Acta Pharmacol Sin* 2018;**39**:1284–93.
56. Zhang X, Liu S, Zhang C, Zhang S, Yue Y, Zhang Y, et al. The role of AMPK $\alpha$ 2 in the HFD-induced nonalcoholic steatohepatitis. *Biochim Biophys Acta Mol Basis Dis* 2020;**1866**:165854.
57. Dokladny K, Myers OB, Moseley PL. Heat shock response and autophagy—cooperation and control. *Autophagy* 2015;**11**:200–13.
58. Horman S, Vertommen D, Heath R, Neumann D, Mouton V, Woods A, et al. Insulin antagonizes ischemia-induced Thr172 phosphorylation of AMP-activated protein kinase  $\alpha$ -subunits in heart via hierarchical phosphorylation of Ser485/491. *J Biol Chem* 2006;**281**:5335–40.
59. Kido K, Yokokawa T, Ato S, Sato K, Fujita S. Effect of resistance exercise under conditions of reduced blood insulin on AMPK $\alpha$  Ser485/491 inhibitory phosphorylation and AMPK pathway activation. *Am J Physiol Regul Integr Comp Physiol* 2017;**313**:R110–9.
60. Singh R, Kaushik S, Wang Y, Xiang Y, Novak I, Komatsu M, et al. Autophagy regulates lipid metabolism. *Nature* 2009;**458**:1131–5.
61. Shimano M, Ouchi N, Shibata R, Ohashi K, Pimentel DR, Murohara T, et al. Adiponectin deficiency exacerbates cardiac dysfunction following pressure overload through disruption of an AMPK-dependent angiogenic response. *J Mol Cell Cardiol* 2010;**49**:210–20.
62. Russo SB, Baicu CF, Van Laer A, Geng T, Kasiganesan H, Zile MR, et al. Ceramide synthase 5 mediates lipid-induced autophagy and hypertrophy in cardiomyocytes. *J Clin Invest* 2012;**122**:3919–30.
63. Xu K, Yang Y, Yan M, Zhan J, Fu X, Zheng X. Autophagy plays a protective role in free cholesterol overload-induced death of smooth muscle cells. *J Lipid Res* 2010;**51**:2581–90.
64. Fabbri E, Magkos F. Hepatic steatosis as a marker of metabolic dysfunction. *Nutrients* 2015;**7**:4995–5019.
65. Tilg H, Moschen AR. Evolution of inflammation in nonalcoholic fatty liver disease: the multiple parallel hits hypothesis. *Hepatology* 2010;**52**:1836–46.